Struct Multidisc Optim (2016) 54:95–116
DOI 10.1007/s00158-015-1390-1

RESEARCH PAPER

Filtering structures out of ground structures – a discrete filtering tool for structural design optimization

Adeildo S. Ramos Jr.[1] · **Glaucio H. Paulino**[2]

Received: 12 May 2015 / Revised: 5 December 2015 / Accepted: 7 December 2015 / Published online: 25 January 2016

Abstract This paper presents an efficient scheme to filter structures out of ground structures, which is implemented using a nested elastic formulation for compliance minimization. The approach uses physical variables and allows control of the minimum ratio between the minimum and maximum areas in the final topology. It leads to a singular problem which is solved using a Tikhonov regularization on the structural problem (rather than on the optimization problem). The filter allows a multiple choice solution in which the user can control the global equilibrium residual in the final structural topology and limit variations of the objective function between consecutive iterations (e.g., compliance). As a result, an unambiguous discrete solution is obtained where all the bars that belong to the topology have well-defined finite areas. This filter feature, with explicit control of member areas, allows the user (e.g., engineer or architect) to play with different alternatives prior to selecting a specific structural configuration. Examples are provided to illustrate the properties of the present approach and the fact that the technique does not always lead to a fully stressed design. The method is efficient in the sense that the finite element solution is computed on the filtered structure (reduced order model) rather than on the full ground structure.

Keywords Ground structures · Filter · Topology optimization · Potential energy · Least Squares · Tikhonov regularization · Generalized inverse · Pseudo inverse

✉ Glaucio H. Paulino
paulino@gatech.edu

[1] Federal University of Alagoas, Maceió, AL, Brazil

[2] School of Civil and Environmental Engineering, Georgia Institute of Technology, 790 Atlantic Drive, Atlanta, GA 30332-0355, USA

1 Introduction

We present a discrete (as opposed to continuum) filtering scheme, which is applicable to ground structures composed of truss networks. The key idea consists of filtering structures out of ground structures so that we obtain clearly defined structures during the topology optimization process. Here we concentrate on compliance minimization using a nested elastic formulation (see, for example, Christensen and Klarbring 2009 and Ohsaki 2011). The motivation for such filtering scheme is outlined below.

The conventional elastic formulation for compliance minimization considers a filter at the end of the optimization process, in which a lower bound is selected for the minimum member areas, i.e., $x_j^{\min} = \epsilon > 0$, j = 1, …, n where n is the number of bars of the ground structure (see Appendix A for Nomenclature). When using this approach, bars that have cross sectional area equal to ϵ are deleted when the optimal solution that defines the topology is obtained. According to Christensen and Klarbring (2009), this sounds simple, however, it also introduces peculiarities in the solution as it can be cumbersome to find a proper value for ϵ. For instance, if ϵ is too small, then there will be undesirable thin bars in the final solution and, in addition, the stiffness matrix will be ill-conditioned. On the other hand, if ϵ is too large, then bars that are structurally important might be deleted and global equilibrium may not be satisfied. Thus application of the filter at the end of the optimization process can lead to undesirable thin bars and/or violation of equilibrium. This situation is illustrated by the simple example of Fig. 1. The corresponding results are shown in Fig. 2 where Fig. 2a illustrates a situation where a proper ϵ is chosen and Fig. 2b illustrates a situation where global equilibrium is violated.

As a further motivation to this work, it is worth investigating what happens if there is no filter at all in the process.

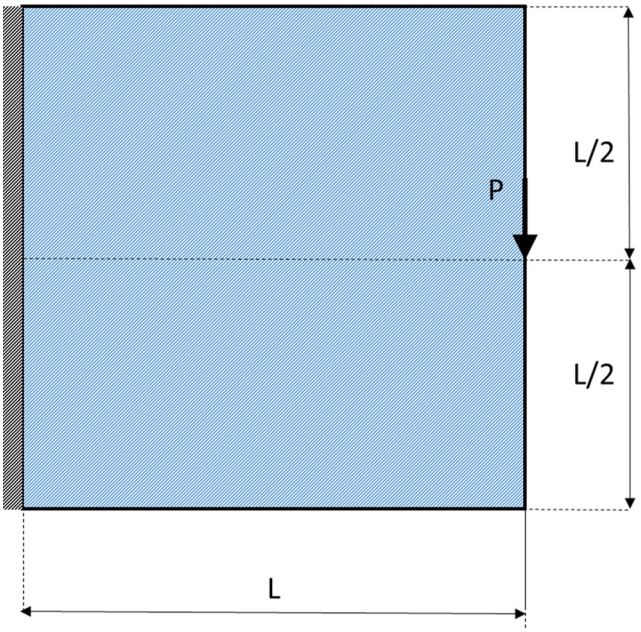

Fig. 1 Design domain where the ground structure (GS) is defined

Figure 3a illustrates the results without filter using the conventional elastic formulation for compliance minimization with an arbitrarily low cross-sectional area selected as, for example, $x^{min} = 5.91\ 10^{-13}\ m^2$. Notice that, in this case, the entire ground structure is obtained as part of the solution and there are many bars with small areas in the final topology. On the other hand, Fig. 3b illustrates results considering $x^{min} = 0\text{-}m^2$, which leads to a singular stiffness matrix. In this case, the equilibrium solution was obtained by means of the potential energy approach with Tikhonov regularization (TR), however, similar solutions could be obtained with a pseudoinverse (Bruns 2006) or iterative solvers (Washizawa et al. 2004; Wang et al. 2007). Even though $x^{min} = 0\ m^2$, not all the cross sectional areas of thin members go to zero, i.e., there are many bars of small area in the final topology. Such examples justify the adoption of an effective filtering scheme to filter structures out of ground structures. The adopted filtering scheme allows enforcement of the global equilibrium and structural resolution (ratio between the minimum and maximum member areas in the topology) while also allowing control of the variation of the objective function between consecutive nonlinear iterations. This leads to a well-defined topology in which all structural members have a finite area. Such approach with member sizing control can also be found in some additive manufacturing publications (Gaynor et al. 2014; Ge et al. 2013; Zegard and Paulino 2015). This filtering scheme is the main contribution of this paper.

The ability to deal with singular systems is important in its own merit (Ben-Israel and Greville 2003) and is employed here to identify non-equilibrium solutions during the filtering process. As shown by Achtziger (1997), the compliance problem is convex even when the stiffness matrix is singular. The filter requires the solution of a singular problem, which is solved using a Tikhonov regularization on the structural problem (rather than on the formal optimization problem). For instance, Fig. 4 illustrates a singular structure displaying members with aligned hinges, which was filtered out of the ground structure. Another situation (not illustrated by Fig. 4) is the appearance of non-connected (or floating) members. The need to solve singular systems is further motivated by Fig. 5, which shows a self-equilibrated initial ground structure; and by Fig. 6, which shows a self-equilibrated filtered structure. It is also useful when dealing with ill conditioned systems that might arise when a thin member (small area) is connected to a thick member (large area) – see Appendix B.

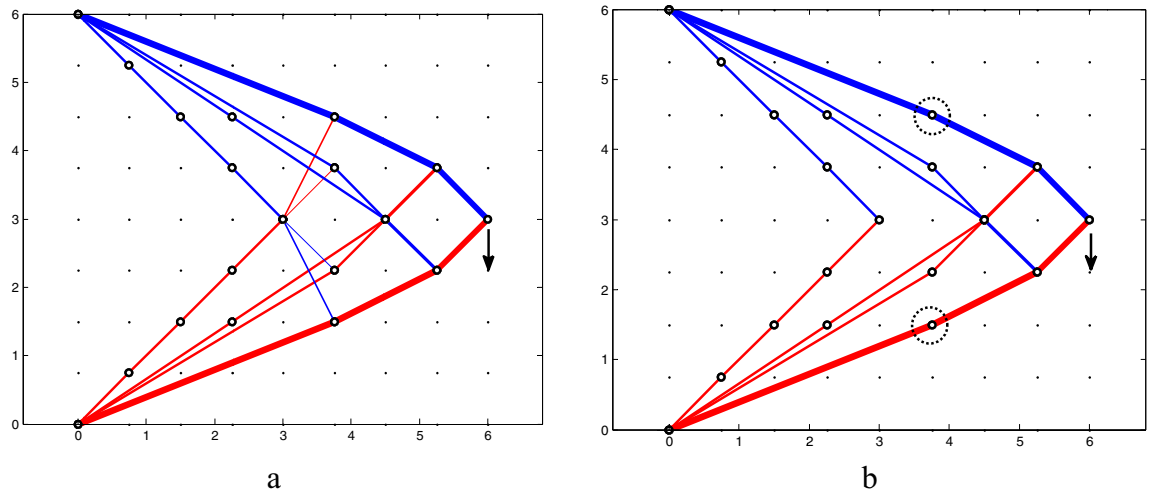

Fig. 2 Conventional elastic formulation using different filter levels: **a** Global equilibrium holds; **b** Global equilibrium does not hold (notice that each circled node is not collinear with its adjacent nodes, leading to a mechanism). *Blue denotes bars* in tension and *red denotes bars* in compression

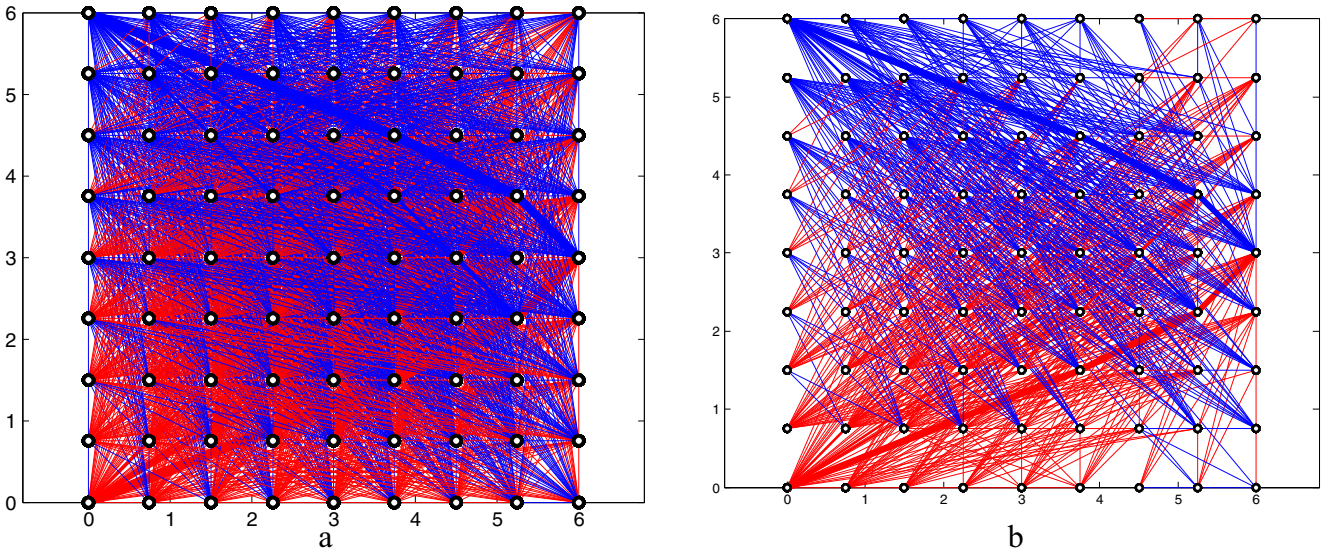

Fig. 3 Results without filter: **a** Conventional approach considering a relatively small lower bound (($x^{min} = 5.91\ 10^{-13}\ m^2$); **b** Singular approach with zero lower bound ($x^{min} = 0$) where the initial ground structure has 2008 members and the final topology illustrated above has 814 members with non-null area. *Blue denotes bars* in tension and *red denotes bars* in compression

As inferred from the aforementioned discussion, the proposed filtering scheme allows well-defined structures to be filtered out of ground structures during the topology optimization process. Thus the problem of small member areas (see, for example, Christensen and Klarbring 2009 and Ohsaki 2011) is solved. In addition, the resolution of the structural topology can be controlled by the user by specifying the minimum ratio between the minimum and maximum areas ($\alpha_f = \min(\boldsymbol{x})/\max(\boldsymbol{x})$). Some advantages of the present filtering scheme include:

- Global equilibrium is enforced by checking the global equilibrium residual
- The user can control the variation of the objective function between consecutive iterations (compliance)
- It leads to efficient solutions because smaller structures (avoiding arbitrarily small member areas) are extracted out of the ground-structure. In this sense, the filter is essentially a reduced order model (of the ground structure).
- It provides an additional degree of freedom to the analyst/designer – different filtering levels lead to different structural realizations (which satisfy global equilibrium).
- The relative sizing of members can be controlled (the filtering level is specified by the user), which provides an indirect means to control the number of members.

The remainder of this paper is organized as follows. Section 2 presents the adopted topology optimization formulation, including a flowchart illustrating our discrete filtering philosophy. Section 3 addresses the sensitivity analysis for the present approach. Section 4 presents numerical examples in which the filtered topologies are in equilibrium (i.e., equilibrium residual is below a certain tolerance) and which also allow control of the variation in the objection function (the latter being an optional parameter). Finally Section 5 presents concluding remarks and potential extensions of this work. Four appendices (A through D) complement the manuscript.

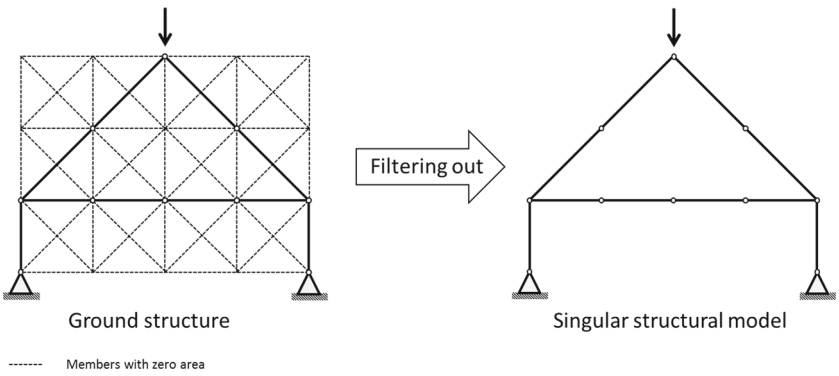

Fig. 4 Filtering out the structural model from the ground structure. The structural model is singular because of the aligned hinges; however, it satisfies global equilibrium

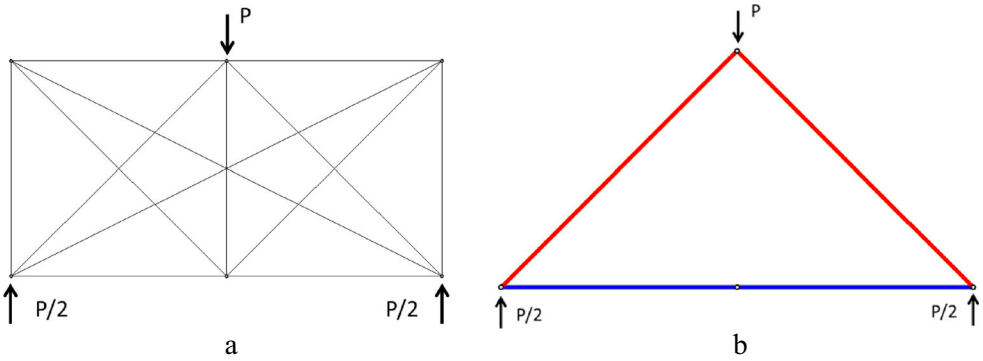

Fig. 5 **a** Self-equilibrated ground structure; **b** filtered structure. *Blue denotes bars* in tension and *red denotes bars* in compression

2 Optimization formulations

For comparison purposes, we first present the standard topology optimization formulation (nested elastic) and then the proposed one. Both formulations consist of determining the cross sectional areas of the truss members using a ground structure (GS) approach. In the standard formulation, there is no clear definition of the structural topology, while in the new formulation there is.

2.1 Standard formulation

We consider the following nested formulation for the optimization problem:

$$\begin{cases} \min\limits_{\boldsymbol{x}} C(\boldsymbol{x}) = \boldsymbol{F}^T \boldsymbol{u}(\boldsymbol{x}) \\ \qquad s.t. \qquad \begin{cases} \boldsymbol{L}^t \boldsymbol{x} - V_{max} \leq 0 \\ 0 < \epsilon = x_j^{min} \leq x_j \leq x_j^{max},\ j = 1, \ldots, n \end{cases} \end{cases}$$
with
$$\boldsymbol{K}(\boldsymbol{x})\boldsymbol{u} = \boldsymbol{F} \tag{1}$$

where $C(\boldsymbol{x})$ is the objective function, $\boldsymbol{x}$ and $\boldsymbol{L}$ are the vectors of area and length, respectively, V_{max} is the maximum material volume, ϵ is a small positive number, and x_j^{min} and x_j^{max} denote the lower and upper bounds for the areas, respectively. The algorithm corresponding to the formulation (1) is shown in Fig. 7. The members which belong to the final topology are defined at the end of the optimization process and these areas satisfy the following criterion:

$$\frac{x_n}{\max(\boldsymbol{x})} \geq \alpha_f \tag{2}$$

where $\alpha_f < 1$ is a non-dimensional parameter and n is the member number, as illustrated by Figs. 8 and 9. From a practical point of view, α_f is usually adopted in the range of 1 %.

2.2 Filter formulation

Rather than regularizing the optimization problem, we choose to regularize the structural problem. Thus we apply the Tikhonov regularization (TR) to the total potential energy in order to solve a singular structural

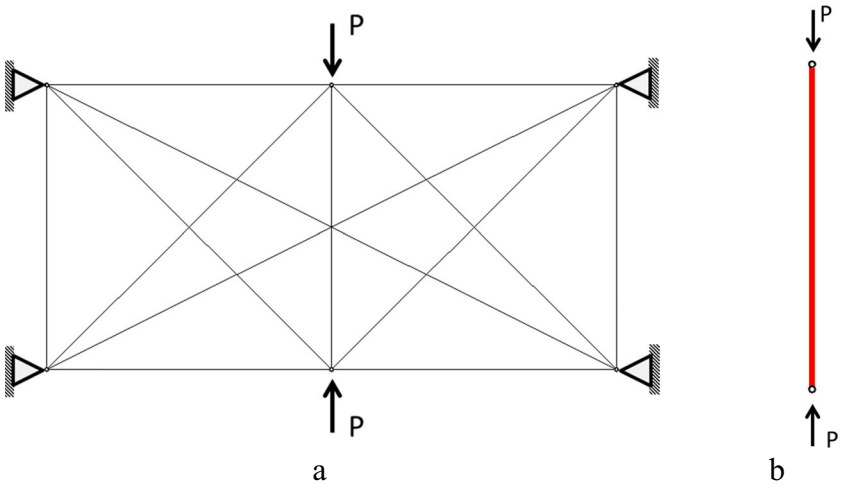

Fig. 6 **a** Ground structure; **b** filtered structure

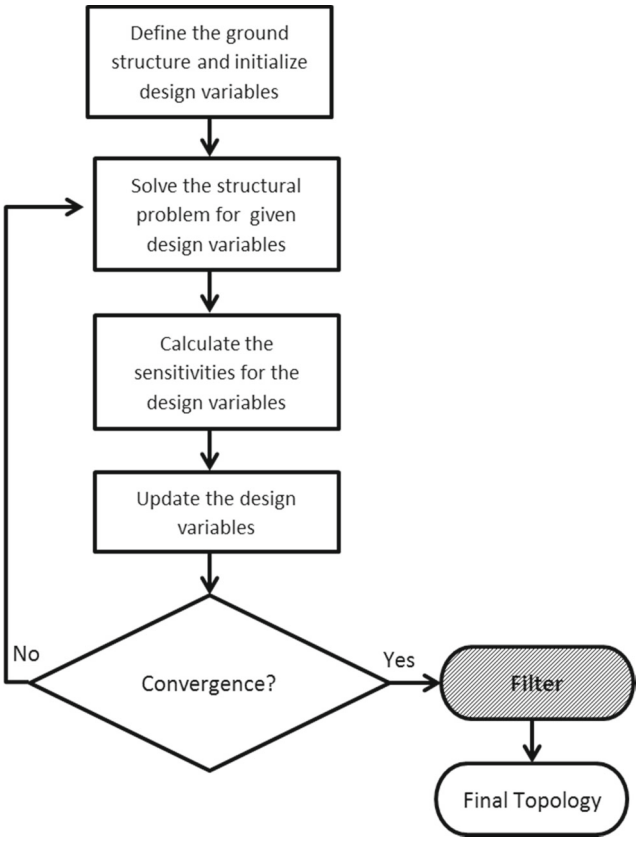

Fig. 7 Standard topology optimization approach – notice that the filter is applied just once at the end of the process

problem. The regularized formulation for the optimization problem is given by:

$$\begin{cases} \min\limits_{\boldsymbol{x}} C(\boldsymbol{x}) = \boldsymbol{F}^T \boldsymbol{u}(\boldsymbol{x}) \\ \qquad s.t. \qquad \begin{cases} \boldsymbol{L}^t \boldsymbol{x} - V_{max} \leq 0 \\ 0 \leq x_j \leq x_j^{max},\ j = 1, \ldots, n \end{cases} \end{cases} \text{with} \quad \boldsymbol{x} = Filter(\boldsymbol{x}, \alpha_f) \quad \text{and} \quad \min_{\boldsymbol{u}} \Pi(\boldsymbol{x}, \boldsymbol{u}(\boldsymbol{x})) + \frac{\lambda}{2} \boldsymbol{u}^T \boldsymbol{u} \tag{3}$$

where Π denotes the potential energy of the system, λ is the Tikhonov regularization parameter, and the proposed *Filter* is defined by

$$Filter(\boldsymbol{x}, \alpha_f) = \begin{cases} 0 & if \ \dfrac{x_n}{\max(\boldsymbol{x})} < \alpha_f < 1 \\ x_n & otherwise \end{cases} \tag{4}$$

and illustrated by Fig. 8.

In this case, the structural topology is defined by the members with non-null areas. The parameter α_f can assume different values and thus allows the user to control

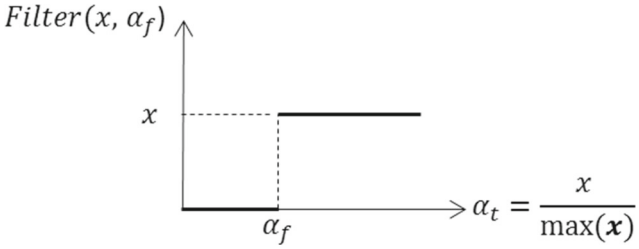

Fig. 8 Filter

the final resolution of the topology, which is defined by the parameter α_{Top}, given by

$$\alpha_{Top} = \frac{\min(\boldsymbol{x}_{Top})}{\max(\boldsymbol{x}_{Top})} \geq \alpha_f \tag{5}$$

where $\boldsymbol{x}_{Top}$ is the vector of member areas which belong the final topology. The corresponding flowchart for the formulation shown in (3) is given by Fig. 10, where $\Delta C(\boldsymbol{x}) = C(\boldsymbol{x}^{k+1}) - C(\boldsymbol{x}^k)$ denotes the increment of the objective function.

2.3 Filtering out

To solve the structural problem, we filter out the topology from the ground structure (see Fig. 4) based on the following mapping of variables:

$$\boldsymbol{u} = \boldsymbol{T}\, \boldsymbol{u}_{Top} \tag{6}$$

The matrix $\boldsymbol{T}$ maps the degrees of freedom between the ground structure ($\boldsymbol{u}$) and the actual topology ($\boldsymbol{u}_{Top}$). This matrix is defined based on the nodes connected to elements of finite area (larger than zero) and loaded nodes with respect to the new set of degrees freedom associated

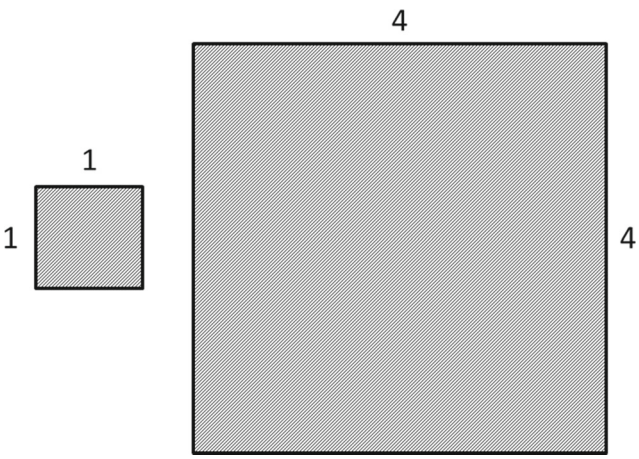

Fig. 9 Illustration of the filter with $\alpha_f = 1/16 = 0.06$

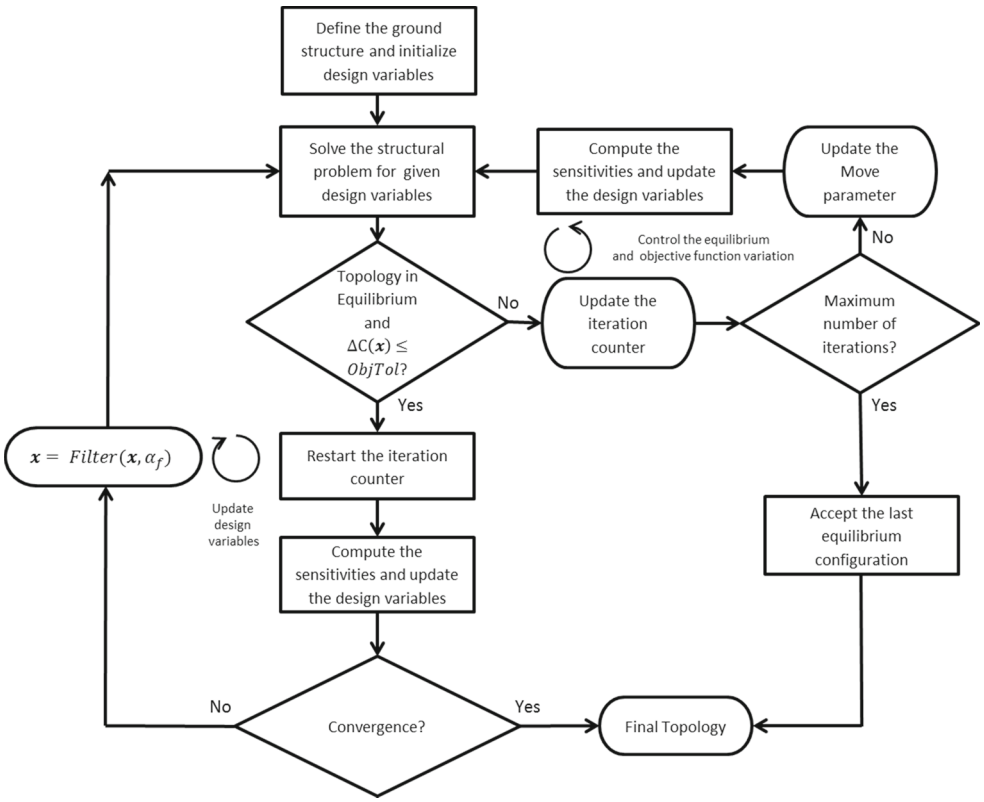

Fig. 10 Flowchart to filter a structure out of the ground structure – the technique provides a structural topology in equilibrium and allows control on the variation of the objective function between consecutive iterations (*ObjTol*)

with them (see Fig. 4 and Appendix D). Based on this mapping, we establish the associated structural problem

$$\boldsymbol{K}_{Top}\boldsymbol{u}_{Top} = \boldsymbol{F}_{Top} \tag{7}$$

where $\boldsymbol{K}_{Top}$ and $\boldsymbol{F}_{Top}$ are the stiffness and load vector respectively associated with the actual topology, which are defined by

$$\boldsymbol{K}_{Top} = \boldsymbol{T}^T \boldsymbol{K}\, \boldsymbol{T} \tag{8}$$

and

$$\boldsymbol{F}_{Top} = \boldsymbol{T}^T \boldsymbol{F} \tag{9}$$

As illustrated by Figs. 4 to 6, the structural problem defined by (7) can be singular and thus we need to check the equilibrium condition (see Appendix B for the near-singular case). In other words, we need to verify if the load vector $\boldsymbol{F}_{Top}$ is in the range of $\boldsymbol{K}_{Top}$ (i. e. $\boldsymbol{F}_{Top} \in \mathscr{R}(\boldsymbol{K}_{Top})$). As indicated above, to solve the singular problem, we minimize the potential energy with Tikhonov regularization. After solving for $\boldsymbol{u}_{Top}$, we obtain the displacements on the ground structure ($\boldsymbol{u}$) using (6). This displacement field is used to calculate the sensitivity on the actual ground structure (see Section 4).

For the sake of simplicity of notation, we drop the subscript (*Top*) from (7) and rewrite it as the following linear system:

$$\boldsymbol{K}\boldsymbol{u} = \boldsymbol{F} \tag{10}$$

where $\boldsymbol{K} \in \mathbb{R}^{n \times n}$ is a symmetric semi-definite stiffness matrix with rank $r \leq n$, and $\boldsymbol{u}$ and $\boldsymbol{F}$ are the displacement and force vectors defined on the structural topology, respectively. The general solution of the system (10) (Ben-Israel and Greville 2003) is given by

$$\boldsymbol{u} = \boldsymbol{u}_p + \boldsymbol{u}_h \tag{11}$$

The terms $\boldsymbol{u}_p$ and $\boldsymbol{u}_h$ are the particular and homogeneous solutions, respectively, of the system (10). The particular solution is of special relevance in the optimization process because it is associated with non-null energies modes and the sensitivities depend on this term only and thus are not impacted by the homogeneous solution (considering that equilibrium holds) – this aspect is addressed in the next section. Below we discuss techniques to obtain the solution of interest. We investigate several alternatives, namely generalized inverses, least squares with Tikhonov regularization and potential energy with Tikhonov regularization, the latter being the method of choice in this work. These alternatives are compared with respect to their ability to identify relevant features of the singular system of equations in connection with their physical interpretation, as discussed below.

2.4 Addressing singular problems

This section address singular solutions, which represents the cornerstone of the present development. First, we address generalized inverses, namely the reflexive inverse and the Moore-Penrose inverse. Then we address Tikhonov regularization approaches, namely least squares and potential energy, the latter being the method of choice in this work.

2.4.1 Generalized inverses

The aforementioned system (10) has solution if

$$\boldsymbol{N}^T\boldsymbol{F} = 0 \tag{12}$$

where $\boldsymbol{N}\in\mathbb{R}^{n\times m}$ is a rectangular matrix whose columns form an m dimensional base of null space of $\boldsymbol{K}(\in\mathbb{R}^{n\times n})$. The general solution of the system (10) is given by (see, for example, Ben-Israel and Greville 2003; Farhat and Géradin 1998)

$$\boldsymbol{u} = \boldsymbol{u}_p + \boldsymbol{u}_h = \boldsymbol{K}^{-}\boldsymbol{F} + (\boldsymbol{I}-\boldsymbol{K}^{-}\boldsymbol{K})\boldsymbol{t} = \boldsymbol{K}^{-}\boldsymbol{F} + \boldsymbol{N}\,\boldsymbol{t} \tag{13}$$

where $\boldsymbol{K}^{-}$ is a generalized inverse of $\boldsymbol{K}$, $\boldsymbol{t}\in\mathbb{R}^m$ is a vector of arbitrary constants, and $\boldsymbol{I}$ is the identity matrix. The terms $\boldsymbol{u}_p=\boldsymbol{K}^{-}\boldsymbol{F}$ and $\boldsymbol{u}_h=\boldsymbol{N}\,\boldsymbol{t}$ are the particular and homogeneous solution, respectively, of the system (10).

Remark 1 Using (13), the compliance $C(\boldsymbol{x})$ can be obtained by

$$C(\boldsymbol{x}) = \boldsymbol{F}^T\boldsymbol{u} = \boldsymbol{F}^T\boldsymbol{K}^{-}\boldsymbol{F} + \boldsymbol{F}^T\boldsymbol{N}\,\boldsymbol{t} \tag{14}$$

If the equilibrium condition holds (see (12)), the compliance is defined only by the particular solution

$$C(\boldsymbol{x}) = \boldsymbol{F}^T\boldsymbol{u}_p \tag{15}$$

Remark 2 In general, the generalized inverse is not unique and can be used for non-square matrices that satisfy the relationship $\boldsymbol{K}\boldsymbol{K}^{-}\boldsymbol{K}=\boldsymbol{K}$. The Moore-Penrose inverse, denoted $\boldsymbol{K}^{+}$, is a stricter generalized inverse that satisfies the following three additional relationships: $\boldsymbol{K}^{-}\boldsymbol{K}\boldsymbol{K}^{-}=\boldsymbol{K}^{-}$; $(\boldsymbol{K}\boldsymbol{K}^{-})^T=\boldsymbol{K}\boldsymbol{K}^{-}$; and $(\boldsymbol{K}^{-}\boldsymbol{K})^T=\boldsymbol{K}^{-}\boldsymbol{K}$ (Ben-Israel and Greville 2003).

Generalized (Reflexive) inverse: $\boldsymbol{K}^{-}$ If we partition $\boldsymbol{K}$ as shown

$$\boldsymbol{K} = \begin{bmatrix} \boldsymbol{K}_{11} & \boldsymbol{K}_{12} \\ \boldsymbol{K}_{21} & \boldsymbol{K}_{22} \end{bmatrix} \tag{16}$$

such that $\boldsymbol{K}_{11}$ is an $r\times r$ submatrix of rank r, then we obtain the generalized (reflexive) inverse by (Ben-Israel and Greville 2003; Farhat and Géradin 1998; Yanai et al. 2011):

$$\boldsymbol{K}^{-} = \begin{bmatrix} \boldsymbol{K}_{11}{}^{-1} & 0 \\ 0 & 0 \end{bmatrix} \tag{17}$$

where the particular solution is given by

$$\boldsymbol{u}_p = \boldsymbol{K}^{-}\boldsymbol{F} \tag{18}$$

Moore-Penrose inverse: $\boldsymbol{K}^{+}$ The particular solution of interest can be obtained using a special class of the generalized inverse, called pseudo-inverse or Moore-Penrose inverse ($\boldsymbol{K}^{+}$), which is obtained using the singular value decomposition (SVD). *In this case, the particular solution is also the minimum norm solution of* $\boldsymbol{u}$ (Ben-Israel and Greville 2003). In general, the SVD solution is computationally expensive, especially for large scale topology optimization problems (Bruns 2006). Alternatively, iterative methods can be used for the solution of singular problems in topology optimization problems (Washizawa et al. 2004). Using the SVD approach for the particular case of symmetric positive semi-definite square matrices with rank r, we obtain (Ben-Israel and Greville 2003)

$$\boldsymbol{K} = \boldsymbol{V}\boldsymbol{S}\boldsymbol{V}^T \tag{19}$$

where $\boldsymbol{S}$ is a diagonal matrix of the singular values, i.e., $\boldsymbol{S}=diag(\sigma_1,\sigma_2,\ldots,\sigma_r,0\ldots,0)$ ordered with $\sigma_1\geq\sigma_2\ldots\geq\sigma_r>0$ and $\boldsymbol{V}$ are a square $n\times n$ orthogonal matrices. In this particular case, σ_k are the eigenvalues of $\boldsymbol{K}$ and the columns of $\boldsymbol{V}$ are the associated eigenvectors. The generalized inverse is given by

$$\boldsymbol{K}^{+} = \boldsymbol{V}\boldsymbol{S}^{+}\boldsymbol{V}^T \tag{20}$$

where $\boldsymbol{S}^{+}=diag(1/\sigma_1,1/\sigma_2,\ldots,1/\sigma_r,0\ldots,0)$. In such case, we can get the particular solution by

$$\boldsymbol{u}_p = \boldsymbol{u}_{min} = \boldsymbol{K}^{+}\boldsymbol{F} \tag{21}$$

or

$$\boldsymbol{u}_{min} = \boldsymbol{V}\boldsymbol{S}^{+}\boldsymbol{V}^T\boldsymbol{F} = \sum_{i=1}^{r}\frac{\mathbf{v}_i^T\boldsymbol{F}}{\sigma_i}\mathbf{v}_i \tag{22}$$

where $\boldsymbol{u}_{min}$ is the minimum norm solution and $\mathbf{v}_i$ denotes the column i of $\boldsymbol{V}$.

2.4.2 Tikhonov regularization

The Tikhonov-type regularization is a common type of regularization of ill-posed problems (see, for example, Engl et al. 1996, and Tikhonov and Arsenin 1977). Here we investigate

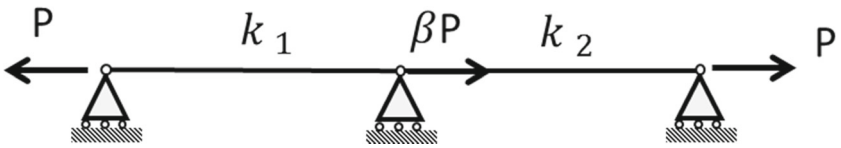

Fig. 11 Structure leading to a singular stiffness matrix: the system is in equilibrium for $\beta=0$ and in non-equilibrium for $\beta\neq 0$. Here the member stiffnesses are $k_1=\frac{20\ kN}{m}$, $k_2=\frac{10\ kN}{m}$ and the load is P = 10 kN

Tikhonov-regularization to address the singularity of a general functional that needs to be regularized:

$$f_r(\boldsymbol{u}) = f(\boldsymbol{u}) + \lambda\, \boldsymbol{u}^T\boldsymbol{u} \tag{23}$$

where λ is the Tikhonov regularization parameter. Below we address the regularization in the context of least squares and potential energy problem statements.

Least squares The particular solution can be obtained using the least squares method with Tikhonov regularization (TR). In this case, we minimize the function given by (Ben-Israel and Greville 2003):

$$\phi(\boldsymbol{u}) = \|\boldsymbol{K}\boldsymbol{u} - \boldsymbol{F}\|^2 + \lambda\, \boldsymbol{u}^T\boldsymbol{u} \tag{24}$$

where $\|*\|$ denotes the Euclidian norm and λ is a small positive number. Minimizing (24), we obtain

$$\boldsymbol{u}_p = \left(\boldsymbol{K}^T\boldsymbol{K} + \lambda\, \boldsymbol{I}\right)^{-1}\boldsymbol{K}^T\boldsymbol{F} \tag{25}$$

Notice that, in this approach, the typical sparsity pattern of the original system is lost. We obtain the Moore-Penrose inverse of $\boldsymbol{K}$ using the following limit approach (Ben-Israel and Greville 2003):

$$\boldsymbol{K}^+ = \lim_{\lambda\to 0}\left(\boldsymbol{K}^T\boldsymbol{K} + \lambda\, \boldsymbol{I}\right)^{-1}\boldsymbol{K}^T \tag{26}$$

and thus the particular solution can be obtained by (21).

Potential energy The particular solution can be obtained by minimizing the total potential energy with Tikhonov regularization (TR). The regularized expression for the potential energy is given by

$$\Pi_R(\boldsymbol{u}) = \Pi(\boldsymbol{u}) + \frac{\lambda}{2}\boldsymbol{u}^T\boldsymbol{u} = \frac{1}{2}\boldsymbol{u}^T\boldsymbol{K}\boldsymbol{u} - \boldsymbol{u}^T\boldsymbol{F} + \frac{\lambda}{2}\boldsymbol{u}^T\boldsymbol{u} \tag{27}$$

where λ is a small positive number as before. In the case of singular $\boldsymbol{K}$ and when there is no solution, the total potential energy $\Pi(\boldsymbol{u})$ becomes unbounded. Minimizing $\Pi_R(\boldsymbol{u})$ (with respect to $\boldsymbol{u}$), we obtain

$$(\boldsymbol{K} + \lambda\, \boldsymbol{I})\boldsymbol{u}_p = \boldsymbol{F} \tag{28}$$

In the examples below, we select the value of λ as $\lambda_o = 10^{-8}$ to 10^{-12} times the mean of the diagonal of $\boldsymbol{K}$.

Considering the spectral decomposition of (28) and using (19) and the orthogonality condition $\boldsymbol{V}\boldsymbol{V}^T=\boldsymbol{I}$, we obtain

$$\left(\boldsymbol{V}\boldsymbol{S}\boldsymbol{V}^T + \lambda\, \boldsymbol{I}\right)\boldsymbol{u}_p = \boldsymbol{V}(\boldsymbol{S} + \lambda\, \boldsymbol{I})\boldsymbol{V}^T\boldsymbol{u}_p = \boldsymbol{F} \tag{29}$$

The particular solution is given by

$$\boldsymbol{u}_p = \boldsymbol{V}(\boldsymbol{S} + \lambda\, \boldsymbol{I})^+\boldsymbol{V}^T\boldsymbol{F} = \sum_{i=1}^{r}\frac{\mathbf{v}_i^T\boldsymbol{F}}{\sigma_i + \lambda}\mathbf{v}_i + \sum_{j=r+1}^{n}\frac{\mathbf{v}_j^T\boldsymbol{F}}{\lambda}\mathbf{v}_j \tag{30}$$

If the force vector $\boldsymbol{F}$ is in the range of $\boldsymbol{K}$ (equilibrium condition holds) than $\mathbf{v}_j^T\boldsymbol{F}=0$ for $j=r+1..n$. Taking the limit in the equation (30), we obtain

$$\boldsymbol{u}_p = \lim_{\lambda\to 0}\sum_{i=1}^{r}\frac{\mathbf{v}_i^T\boldsymbol{F}}{\sigma_i + \lambda}\mathbf{v}_i + \sum_{j=r+1}^{n}\frac{\mathbf{v}_j^T\boldsymbol{F}}{\lambda}\mathbf{v}_j = \begin{cases}\boldsymbol{u}_{min}\ if\ \ \boldsymbol{F}\in\mathscr{R}(\boldsymbol{K})\\ \infty\ if\ \ \boldsymbol{F}\notin\mathscr{R}(\boldsymbol{K})\end{cases} \tag{31}$$

Table 1 Self equilibrated case ($\beta=0$; $k_1=20kN/m$, $k_2=10kN/m$; P = 10 kN)

Method	$\boldsymbol{u}_p(m)$	$C=\boldsymbol{F}^T\boldsymbol{u}_p(kN\ m)$	$\|\boldsymbol{K}\boldsymbol{u}_p-\boldsymbol{F}\|/\|\boldsymbol{F}\|$
Gen. (Reflexive) Inverse	$\{-1.5000\quad -1.0000\quad 0.0000\}^T$	15.00	$3.5527\ 10^{-16}$
Moore-Penrose Inverse	$\{-0.6667\quad -0.1667\quad 0.8333\}^T$	15.00	$3.5527\ 10^{-16}$
Least square + TR	$\{-0.6667\quad -0.1667\quad 0.8333\}^T$	15.00	$4.8074\ 10^{-8}$
Potential Energy + TR	$\{-0.6667\quad -0.1667\quad 0.8333\}^T$	15.00	$1.5275\ 10^{-8}$

Table 2 Non-equilibrium case ($\beta=1$; $k_1=20kN/m$, $k_2=10kN/m$; P = 10 kN)

Method	$\boldsymbol{u}_p(m)$	$C=\boldsymbol{F}^T\boldsymbol{u}_p(kN\ m)$	$\|\boldsymbol{K}\boldsymbol{u}_p-\boldsymbol{F}\|/\|\boldsymbol{F}\|$
Gen. (Reflexive) Inverse	$\{-2.5000\quad -2.0000\quad 0.0000\}^T$	45	0.5774
Moore-Penrose Inverse	$\{-0.6667\quad -0.3333\quad 1.0000\}^T$	20	0.3333
Least square + TR	$\{-0.6667\quad -0.3333\quad 1.0000\}^T$	20	0.3333
Potential Energy + TR	$\{-1.6667\quad -1.6667\quad -1.6667\}^T\ 10^7$	$1.6667\ 10^8$	0.3333

An alternative solution of (28) can be done through an iterative process, as shown in the Appendix C. As indicated above, a proper value λ needs to be chosen in the numerical procedure (24), however, in the iterative process, the solution does not have such explicit dependence on the parameter λ. As expected, the computational cost of the iterative process is higher than the direct solution of (28).

2.5 How to detect non-equilibrium solutions?

We provide the answer to this question by means of the example illustrated by Fig. 11. We check the global equilibrium error by

$$\|\boldsymbol{K}\boldsymbol{u}-\boldsymbol{F}\|\leq\rho\|\boldsymbol{F}\| \tag{32}$$

where ρ is a specified tolerance (e.g., $\rho=10^{-4}$). We obtain numerical results using the generalized (reflexive) inverse, Moore-Penrose inverse, least squares with Tikhonov regularization, and total potential energy with Tikhonov regularization. We employ $\lambda_o=10^{-8}$ and check the global equilibrium error and compliance for each case.

For the structure of Fig. 11, the stiffness matrix is given by

$$\boldsymbol{K}=\begin{bmatrix} k_1 & -k_1 & 0 \\ -k_1 & k_1+k_2 & -k_2 \\ 0 & -k_2 & k_2 \end{bmatrix} \tag{33}$$

and the generalized inverse is given according to (17):

$$\boldsymbol{K}^{-}=\begin{bmatrix} \boldsymbol{K}_{11}{}^{-1} & 0 \\ 0 & 0 \end{bmatrix}=\begin{bmatrix} 0.15 & 0.1 & 0 \\ 0.1 & 0.1 & 0 \\ 0 & 0 & 0 \end{bmatrix} \tag{34}$$

where $\boldsymbol{K}_{11}$ is obtained removing the last line and column of the stiffness matrix (33).

First, we consider a singular and self-equilibrated system (Fig. 11 considering $\beta=0$), and obtain the results shown in Table 1. In this case, we obtain the minimum norm solution for all cases, except for the generalized (reflexive) inverse. The residual in equilibrium is smaller when we do not use Tikhonov regularization but, in all cases, the residual is smaller than the adopted equilibrium tolerance ($\rho=10^{-4}$).

Next, we consider non-equilibrium cases (Fig. 11 considering $\beta\neq0$), which are summarized in Table 2 ($\beta=1$), Table 3 ($\beta=0.1$) and Table 4 ($\beta=0.001$). Here β is a non-equilibrium parameter in the sense that its magnitude measures the deviation from equilibrium. *A comparison of the results in Tables 2 to 4 lead to the important observation that, among the methods presented, the potential energy with Tikhonov regularization displays the highest sensitivity in displacement and compliance, which is useful to identify non-equilibrium configurations* (*See* (31)).

3 Sensitivity analysis

In the present approach, the sensitivity analysis is performed on the ground structure, and not on the filtered structure. We

Table 3 Non-equilibrium case ($\beta=0.1$; $k_1=20kN/m$, $k_2=10kN/m$; P = 10 kN)

Method	$\boldsymbol{u}_p(m)$	$C=\boldsymbol{F}^T\boldsymbol{u}_p(kN\ m)$	$\|\boldsymbol{K}\boldsymbol{u}_p-\boldsymbol{F}\|/\|\boldsymbol{F}\|$
Gen. (Reflexive) Inverse	$\{-1.6000\quad -1.1000\quad 0.0000\}^T$	17.100	0.0705
Moore-Penrose Inverse	$\{-0.6667\quad -0.1833\quad 0.8500\}^T$	15.350	0.0407
Least square + TR	$\{-0.6667\quad -0.1833\quad 0.8500\}^T$	15.350	0.0407
Potential Energy + TR	$-\{1.6667\quad 1.6667\quad 1.6667\}^T 10^6$	$1.6667\ 10^6$	0.0407

Table 4 – Non-equilibrium case ($\beta = 0.001$; $k_1 = 20kN/m$; $k_2 = 10kN/m$; P = 10 kN)

Method	$\boldsymbol{u}_p(m)$	$C = \boldsymbol{F}^T\boldsymbol{u}_p(kN\ m)$	$\|\boldsymbol{K}\boldsymbol{u}_p - \boldsymbol{F}\|/\|\boldsymbol{F}\|$
Gen. (Reflexive) Inverse	$\{1.5010 \quad 1.0010 \quad 0.0000\}^T$	15.0200	$7.0711\ 10^{-4}$
Moore-Penrose Inverse	$\{0.6667 \quad 0.1668 \quad -0.8335\}^T$	15.0033	$4.0825\ 10^{-4}$
Least square + TR	$\{0.6667 \quad 0.1668 \quad -0.8335\}^T$	15.0033	$4.0825\ 10^{-4}$
Potential Energy + TR	$\{1.6667 \quad 1.6667 \quad 1.6666\}^T\ 10^4$	181.670	$4.0825\ 10^{-4}$

assume that the ground structure has an associated structural model in equilibrium, in other words, the gradient of the total potential energy is zero $\left(\partial\Pi(\boldsymbol{x},\boldsymbol{u}(\boldsymbol{x}))/\partial\boldsymbol{u}|_{\boldsymbol{u}=\boldsymbol{u}_{eq}} = 0\right)$, where $\boldsymbol{u}_{eq}$ denotes the displacement vector at the equilibrium configuration. The relationship between compliance and total potential energy is given by

$$C(\boldsymbol{x}) = \boldsymbol{F}^T\boldsymbol{u}(\boldsymbol{x}) = -2\min_{\boldsymbol{u}}\Pi(\boldsymbol{x},\boldsymbol{u}(\boldsymbol{x})) = -2\,\Pi\left(\boldsymbol{x},\boldsymbol{u}_{eq}(\boldsymbol{x})\right) \tag{35}$$

Thus the sensitivity of compliance is given by

$$\frac{dC(\boldsymbol{x})}{dx_n} = -2\frac{\partial\Pi\left(\boldsymbol{x},\boldsymbol{u}_{eq}(\boldsymbol{x})\right)}{\partial x_n} - 2\frac{\partial\Pi(\boldsymbol{x},\boldsymbol{u}(\boldsymbol{x}))}{\partial\boldsymbol{u}}\bigg|_{\boldsymbol{u}=\boldsymbol{u}_{eq}}\frac{\partial\boldsymbol{u}_{eq}}{\partial x_n} \tag{36}$$

If the equilibrium condition holds (i.e. $\partial\Pi(\boldsymbol{x},\boldsymbol{u}(\boldsymbol{x}))/\partial\boldsymbol{u}|_{\boldsymbol{u}=\boldsymbol{u}_{eq}} = 0$), then we obtain

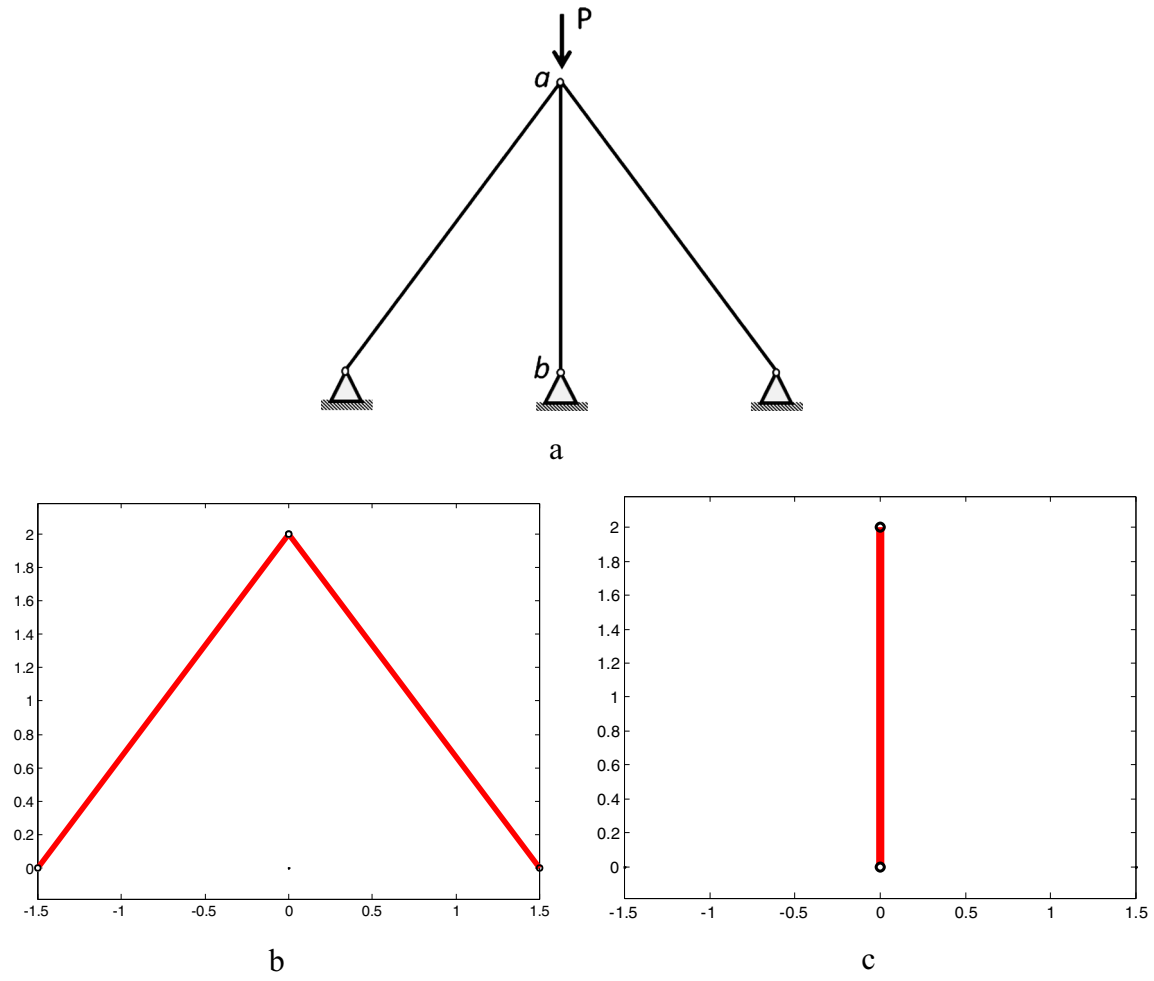

Fig. 12 Restoring a vanished member (i.e., null area) to the structure: **a** Initial condition where member "ab" has zero initial area; **b** Final topology obtained using the OC; **c** Final topology obtained using the MMA (Svanberg 1987)

$$\frac{dC(\boldsymbol{x})}{dx_n} = -2\frac{\partial \Pi\left(\boldsymbol{x}, \boldsymbol{u}_{eq}(\boldsymbol{x})\right)}{\partial x_n} = -2\frac{\partial U\left(\boldsymbol{x}, \boldsymbol{u}_{eq}(\boldsymbol{x})\right)}{\partial x_n} - 2\frac{\partial \Omega\left(\boldsymbol{x}, \boldsymbol{u}_{eq}(\boldsymbol{x})\right)}{\partial x_n} \tag{37}$$

where $\Omega(\boldsymbol{x}, \boldsymbol{u}(\boldsymbol{x}))$ is the potential of the external loads, and $U(\boldsymbol{x}, \boldsymbol{u}(\boldsymbol{x}))$ is the strain energy, which is given by

$$U(\boldsymbol{x}, \boldsymbol{u}(\boldsymbol{x})) = \sum_{k=1}^{N} U_k = \sum_{k=1}^{N} \frac{1}{2} (\boldsymbol{u}_k)^T \boldsymbol{k}_k \boldsymbol{u}_k \tag{38}$$

where $\boldsymbol{u}_k$ and $\boldsymbol{k}_k$ denote the displacement vector and stiffness matrix in local coordinates for the member k, respectively. The local displacement vector $\boldsymbol{u}_k$ is related to the global displacement vector $\boldsymbol{u}$ by the connectivity matrix defined by $\boldsymbol{u}_k = \boldsymbol{A}_k \boldsymbol{u}$ (Christensen and Klarbring 2009). The stiffness matrix of the element $\boldsymbol{k}_k$ in local coordinates is given by

$$\boldsymbol{k}_k = x_k \begin{bmatrix} \boldsymbol{k}_{pp} & \boldsymbol{k}_{pq} \\ \boldsymbol{k}_{qp} & \boldsymbol{k}_{qq} \end{bmatrix}^{(k)} = x_k \boldsymbol{k}_k^0 \tag{39}$$

with $\boldsymbol{k}_{pp} = \boldsymbol{k}_{qq} = -\boldsymbol{k}_{qp} = -\boldsymbol{k}_{pq} = (E/\ell)\boldsymbol{n}\ \boldsymbol{n}^T$, where E is the elastic modulus of the material, ℓ is the length of the member and $\boldsymbol{n}$ is the unit vector associated to and along member k. By means of (38) and (39), we obtain

$$U(\boldsymbol{x}, \boldsymbol{u}(\boldsymbol{x})) = \sum_{k=1}^{N} \frac{1}{2} x_k (\boldsymbol{u}_k)^T \boldsymbol{k}_k^0 \boldsymbol{u}_k \tag{40}$$

Because the potential of the loads is explicitly independent of $\boldsymbol{x}$, i.e., $\Omega(\boldsymbol{x}, \boldsymbol{u}(\boldsymbol{x})) = \Omega(\boldsymbol{u}(\boldsymbol{x})) = -\boldsymbol{u}(\boldsymbol{x})^T \boldsymbol{F}$ (no body

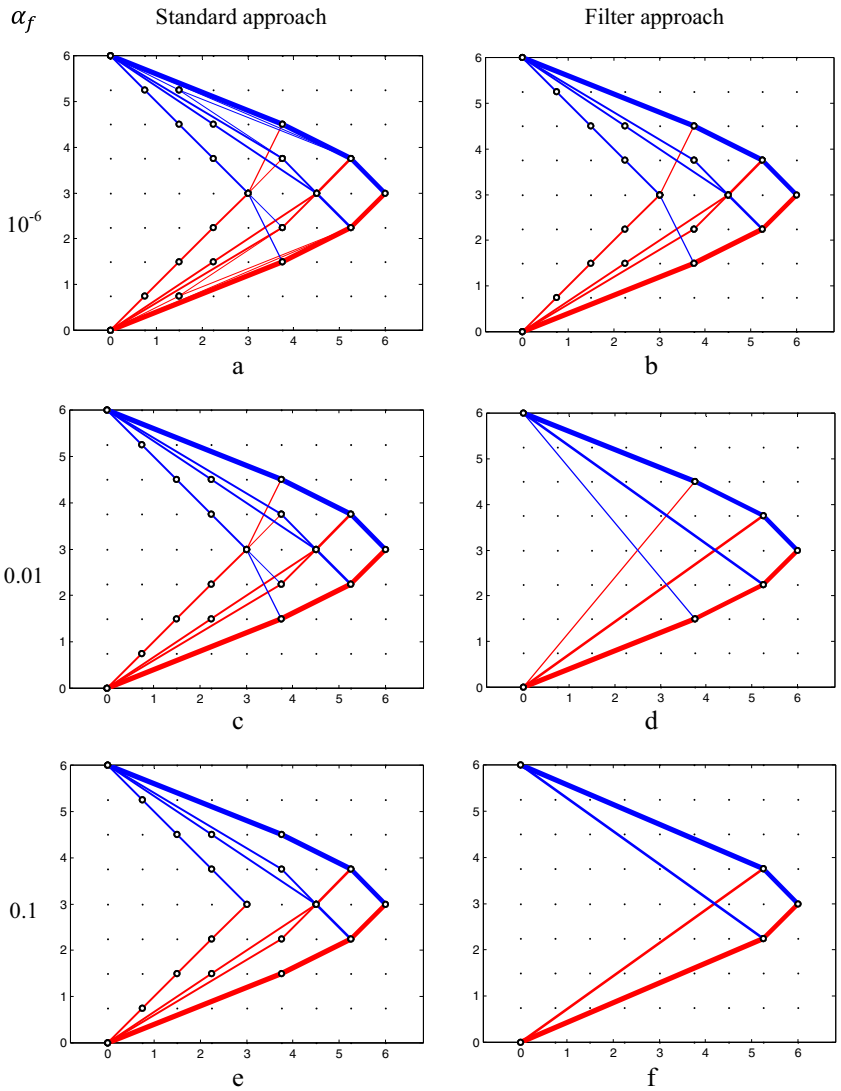

Fig. 13 Results for the standard and new filtering approach. Members in *blue* are in tension and those in *red* are in compression

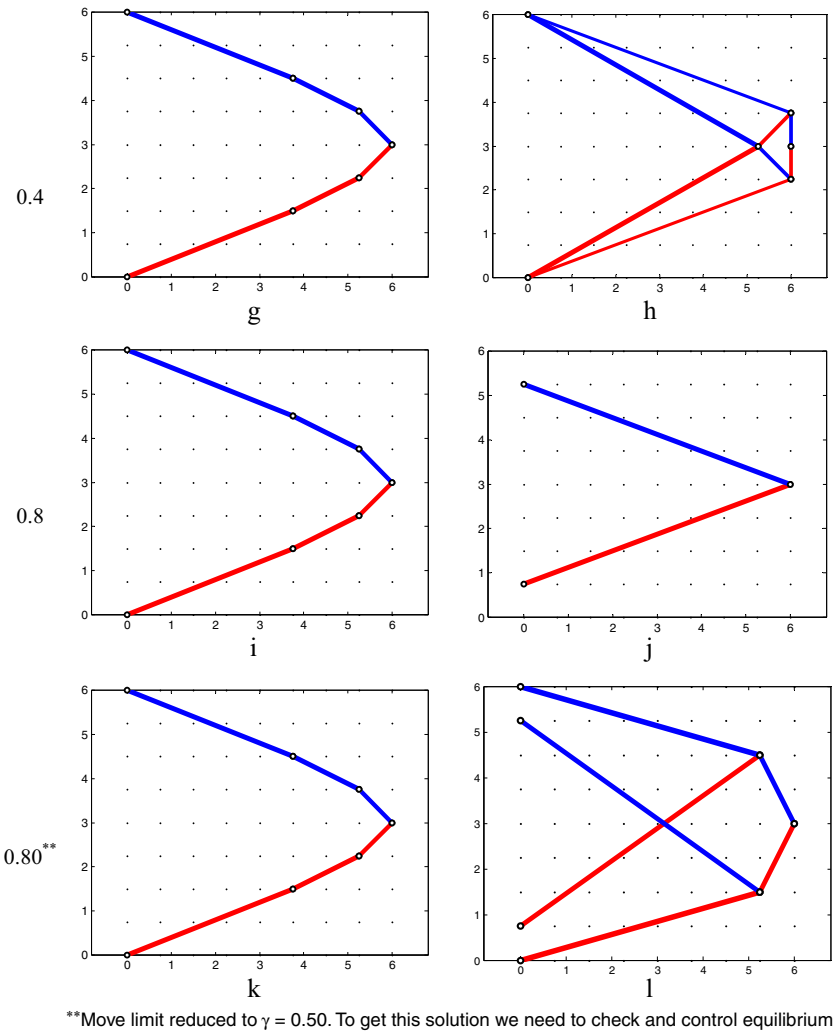

Fig. 13 continued.

forces), then $\partial\Omega(\boldsymbol{x},\boldsymbol{u}(\boldsymbol{x}))/\partial x_n = 0$. Thus, based on (37) and (40), we obtain

$$\frac{dC(\boldsymbol{x})}{dx_n} = -2\frac{\partial U(\boldsymbol{x},\boldsymbol{u}(\boldsymbol{x}))}{\partial x_n} = -(\boldsymbol{u}_n)^T \boldsymbol{k}_n^0 \boldsymbol{u}_n \tag{41}$$

This result shows that the sensitivity is always non positive and independent of the area of the member. This implies that, even members of null area in the ground structure can have a finite sensitivity and thus may return to the topology with a positive area. This feature is illustrated by Fig. 12, which was

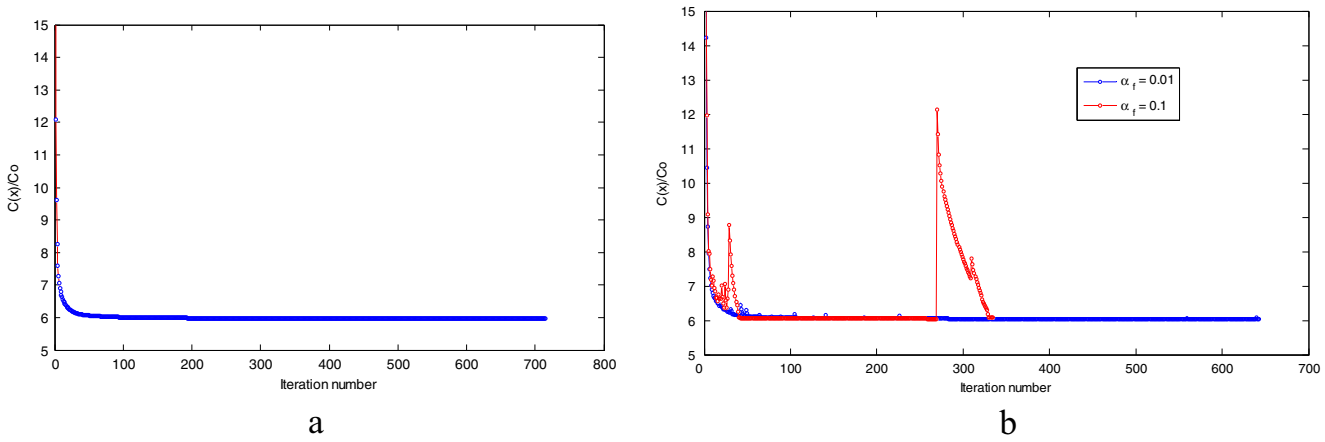

Fig. 14 Objective function: **a** Standard approach; **b** Filter approach with different filtering levels

Table 5 – Representative parameters for Example 1: filter size (α_f), structural topology resolution (α_{Top}), equilibrium residual and compliance values

Formulation	α_f	α_{Top}	$\frac{\|\boldsymbol{K}_{Top}\boldsymbol{u}_{Top}-\boldsymbol{F}_{Top}\|}{\|\boldsymbol{F}_{Top}\|}$	$\overline{C}(\boldsymbol{x}^*)$	$\overline{C}_{Top}(\boldsymbol{x}^*)$
Standard	10^{-6}	$1.11\ 10^{-6}$	–	5.975	≥5.975
	0.01	0.0487	–		≥5.975
	0.10	0.1537	–		–
	0.40	0.9520	–		–
	0.80	0.9520	–		–
	0.80	0.9520	–		–
Filter	10^{-6}	$6.97\ 10^{-4}$	$7.611\ 10^{-8}$	5.975	5.975
	0.01	0.0853	$1.306\ 10^{-7}$	6.038	6.038
	0.10	0.3765	$1.166\ 10^{-7}$	6.072	6.072
	0.40	0.5299	$1.804\ 10^{-7}$	6.597	6.831
	0.80	1.0000	$4.056\ 10^{-8}$	9.251	9.251
	0.80**	0.8000	$7.598\ 10^{-8}$	7.459	7.459

$\overline{C}(\boldsymbol{x}^*) = C(\boldsymbol{x}^*)/C_o$; $\overline{C}_{Top}(\boldsymbol{x}^*) = C_{Top}(\boldsymbol{x}^*)/C_o$; $C_o = P^2\ L^2/E\ V_{max}$; $tol = 10^{-8}$

** Move limit reduced to $\gamma = 0.50$. To get this solution we need to check and control equilibrium

obtained with the method of moving asymptotes (MMA) (Svanberg 1987). However, if the optimality criteria (OC) is used, then the member of null area does not return to the topology (due to the recurring form of the OC which applies a multiplicative factor on the previous area). From a practical point of view, the structural engineer might be mostly interested in relatively lower values of the filter. In this scenario, the return of bars is rather infrequent, and thus the use of the OC might be an acceptable approximation. This is the approach used in this work.

4 Numerical examples

Representative numerical examples are provided to highlight the main features of the proposed filtering scheme. As indicated before, the examples in this paper rely on the optimality criteria (OC) with $\alpha_i = -1 (\eta = 0.5)$ and move limit $M = \gamma\ \boldsymbol{x}_0$ (see Ramos and Paulino 2015; Groenwold and Etman 2008).

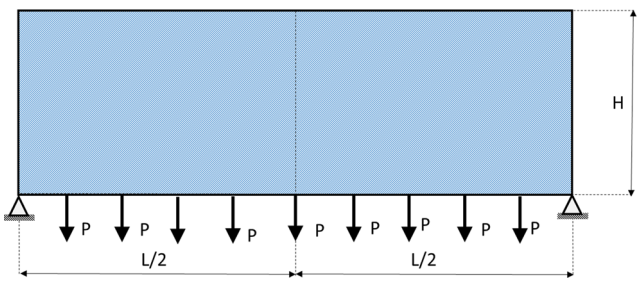

Fig. 15 Idealized bridge problem: geometry (L = 10 m; $H = 5m$), load ($P = 10$ kN), and support conditions. A full level ground structure (11 × 11 grid) is used with 3752 non-overlapped bars ($V_{max} = 0.0056m^3$)

The initial area ($\boldsymbol{x}_0$) of all members is defined as the ratio between the maximum volume (V_{max}) and the sum of the length of all ground structure members. For the standard GS approach (e.g., Christensen and Klarbring 2009), the lower and upper bounds are defined by, for example, $\boldsymbol{x}^{min} = 10^{-4}\boldsymbol{x}_0$ and $\boldsymbol{x}^{max} = 10^4\boldsymbol{x}_0$ ($\boldsymbol{x}_0$ is the vector of initial areas), respectively, and $\gamma = 500$. For the present filtering approach, $\boldsymbol{x}^{min} = 0$ (not a small threshold, as required by the standard formulation), $\boldsymbol{x}^{max} = 10^4\boldsymbol{x}_0$, and γ is defined for each example below. Moreover, Young's modulus $E = 70\ 10^6 kN/m^2$ is the same for all examples.

4.1 Example 1 – Square domain with a concentrated load

This example, which is illustrated by Fig. 1, consists of a square domain with a concentrated load ($P = 70$ kN). A full level ground structure associated to a 9 × 9 grid with 2008 non-overlapped bars (L = 6 m and $V_{max} = 0.004m^3$) is used. Initially, we compare the standard (post-processing) approach with the present filtering approach. To that effect, the same grid is considered with different filter levels (pre-processing stage). For the standard approach, the minimum area is $x_j^{min} = 5.9\ 10^{-13}\ m^2$; while the maximum area is $x_j^{max} = 5.9\ 10^{-3}\ m^2$ for all the approaches. Moreover, $V_{max} = 0.004\ m^3$, the convergence tolerance $tol = 10^{-8}$ and, unless otherwise stated, $\gamma = 5$ (factor associated with the move parameter). A comparison of topologies obtained from both standard and filtering approaches is provided in Fig. 13. While the structures for the standard approach are not necessarily in equilibrium, the ones provided by the filtering approach are guaranteed to be in equilibrium. A comparison of the objective function for both

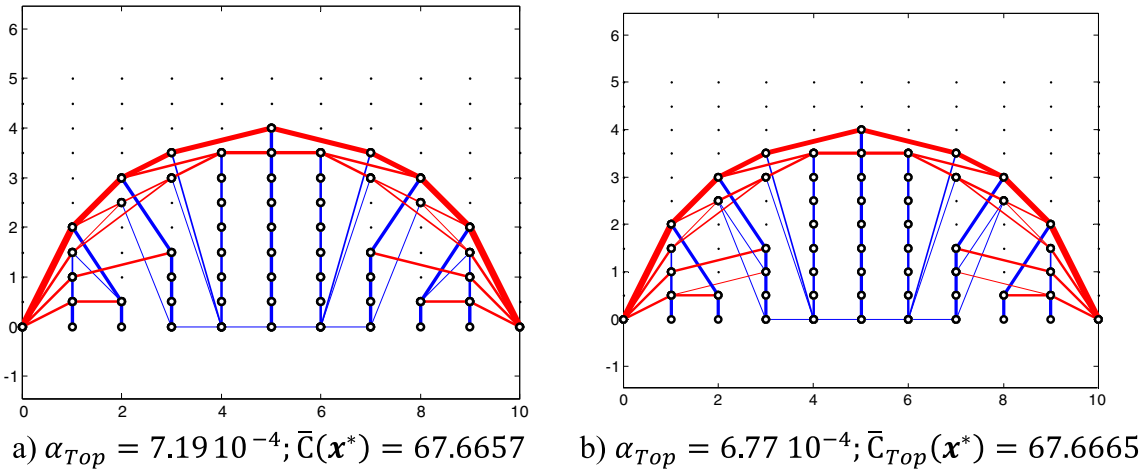

Fig. 16 Topology optimization ($\alpha_f = 10^{-4}$) based on a full ground structure (11 × 11grid) with 3752 members: **a** Standard approach; **b** Filter approach with TR ($\lambda_o = 10^{-8}$) and $\gamma = 4$

approaches is provided in Fig. 14. Notice that Fig. 14b includes 2 values of filters: 0.1 and 0.01. The value of the tolerance for the objective function is basically unlimited (set to be a large number). Thus for the low value of filter, the objective function is smooth and for the higher value of the filter, there are jumps in the objective function (as expected). In summary, for the filtering approach, although there are jumps in the objective function, a converged result is ultimately obtained.

Table 5 presents results associated with the example of Fig. 1. The equilibrium residual in the standard formulation is not provided because the displacement vector $\boldsymbol{u}_{Top}$ is not available in that case (i.e., the topology is not defined). The equilibrium residual in this table confirms that all the topologies obtained with the present filtering scheme are in equilibrium. Moreover, as expected, $\alpha_{\text{Top}} \geq \alpha_{\text{f}}$ (cf. 5).

4.2 Example 2 – Bridge problem

Figure 15 shows an idealized bridge model. We address the computational efficiency of the proposed formulation and discuss the dependency of the solution with respect to the Tikhonov parameter and the move parameter in the OC. In addition, we control the variation of the objective function between successive iterations and investigate the equilibrium state during the solution process. In this problem, the minimum area is: $x_j^{min} = 4.16\,10^{-15}\,m^2$ (standard approach) and the maximum area is: $x_j^{max} = 4.16\ 10^{-3}\ m^2$ (all approaches). Moreover, $V_{max} = 0.0056\ m^3$ and, unless otherwise stated, the convergence tolerance $tol = 10^{-9}$ for this example. In all topology results to follow, blue denotes members in tension and red denotes members in compression. Figure 16 shows the results obtained using an 11×11 grid which composes a ground structure with 3752 members considering $\alpha_f = 10^{-4}$. Figure 16a illustrates the topology obtained with the standard approach, and Fig. 16b with the filter approach using TR ($\lambda_o = 10^{-8}$) and $\gamma = 4$ (factor associated with the move parameter). Both solutions lead to fully stressed designs (FSDs) with absolute axial stress $15.00\ 10^4 kN/m^2$.

Table 6 presents results associated with the example of Fig. 17. The third column of the table indicates the high efficiency of the proposed filtering scheme (filter + TR) with respect to other approaches (Standard and Filter + SVD). The fourth column confirms that, as expected, $\alpha_{\text{Top}} \geq \alpha_{\text{f}}$ (cf. Eq. 5). The last column shows the compliance for each case.

The efficiency of the proposed filtering scheme is further illustrated by Fig. 17 which compares the CPU time for each iteration of the standard approach and the present filtering approach (Filter + TR). Notice that the comparison is made solely for the solution of the resulting structural model. Thus the standard approach includes the time to build the stiffness matrix and to solve the linear system for the actual ground structure. On the other hand, the filter approach extracts the actual structural topology from the ground structure, generates new nodal coordinates and connectivity, builds the reduced stiffness matrix, and solves the regularized linear system. The evolution of the system stiffness matrix is shown in Fig. 17b through d. Notice we start with an initial stiffness

Table 6 Representative parameters for solution with $\alpha_f = 10^{-4}$ and $tol = 10^{-9}$; $\lambda_o = 10^{-8}$

Formulation	Number of Iterations	CPU (s)	α_{Top}	$\bar{C}(x^*)$
Standard	4498	599	7.1910^{-4}	67.6657
Filter + SVD	2637	133	$2.10\ 10^{-3}$	68.7560
Filter + TR	**567**	**35**	$\mathbf{6.77\ 10^{-4}}$	**67.6665**

$\bar{C}(x^*) = C(x^*)/C_o; \bar{C}_{Top}(x^*) = C_{Top}(x^*)/C_o; C_o = P^2\ L^2/E\ V_{max}$

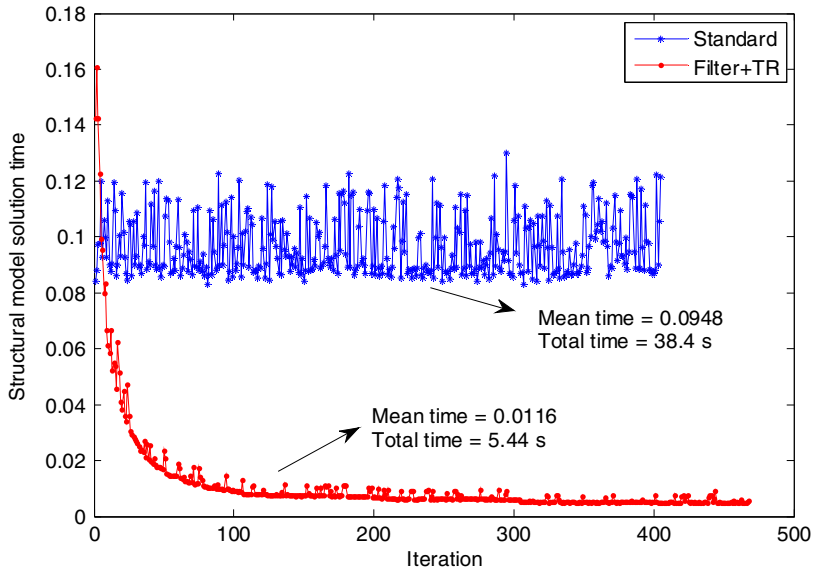

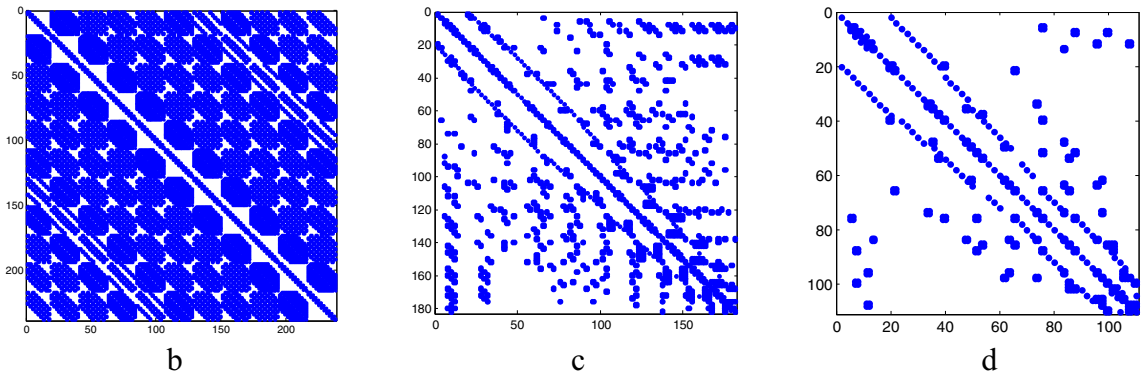

Fig. 17 **a** CPU time for the solution of the structural model during each topology optimization iteration for the problem of Fig. 15 – full ground structure (11 × 11 grid) and $\alpha_f = 10^{-4}$, $tol = 10^{-8}$, $\lambda_o = 10^{-8}$. Notice that $tol = 10^{-8}$ (rather than $tol = 10^{-9}$) was adopted so that both approaches have similar number of iterations. **b** Pattern of the initial stiffness matrix (238 × 238) with 28,556 non null elements; **c** Pattern of the stiffness matrix in the 50th iteration (182 × 182) with 2,997 non null elements; **d** Final pattern of the stiffness matrix with (110 × 110) with 502 non null elements

matrix with 28,556 non-null components (Fig. 17b), which is reduced to 2,997 non-null components in the 50th iteration (Fig. 17c), and to 502 non-null components in the final iteration (Fig. 17d). Thus the comparative efficiency of the present filtering scheme is clear from Fig. 17.

Figure 18 illustrates the dependence of the move size (OC γ parameter) on the topology using the filter approach. Although the topologies are different, they also exhibit some similarities. Comparing Fig. 18a and b, we notice that as the move increases, α_{Top} increases and the compliance decreases. These solutions lead to a FSD with absolute axial stress 15.00 $10^4 kN/m^2$ and 14.90 $10^4 kN/m^2$, respectively.

Figure 19 illustrates the dependence of the Tikhonov parameter (λ_o) on the topology using the filter approach. Although the topologies are different, they also exhibit some similarities. Comparing Fig. 19a and b, we notice that as the Tikhonov parameter is tightened (i.e., reduced), α_{Top} decreases and the compliance increases, which are the opposite trends of the previous example. These solutions lead to a FSD with absolute axial stress 15.00 $10^4 kN/m^2$ and 15.24 $10^4 kN/m^2$, respectively.

Figures 20 and 21 illustrate the filter with TR on a full ground structure (11 × 11 grid) for $\alpha_f = 0.03$ without ($\gamma = 1/4$; $ObjTol = 100$) and with ($\gamma = 1/4$; $ObjTol = 1$) active objective function control, respectively. A comparison of Fig. 20b with Fig. 21b reveals that the former case leads to a FSD, while the latter case does not.

Similarly, Figs. 22 and 23 illustrate the filter with TR on a full ground structure (11 × 11 grid) for $\alpha_f = 0.06$ with objective function control ($\gamma = 5$) and with both objective function and

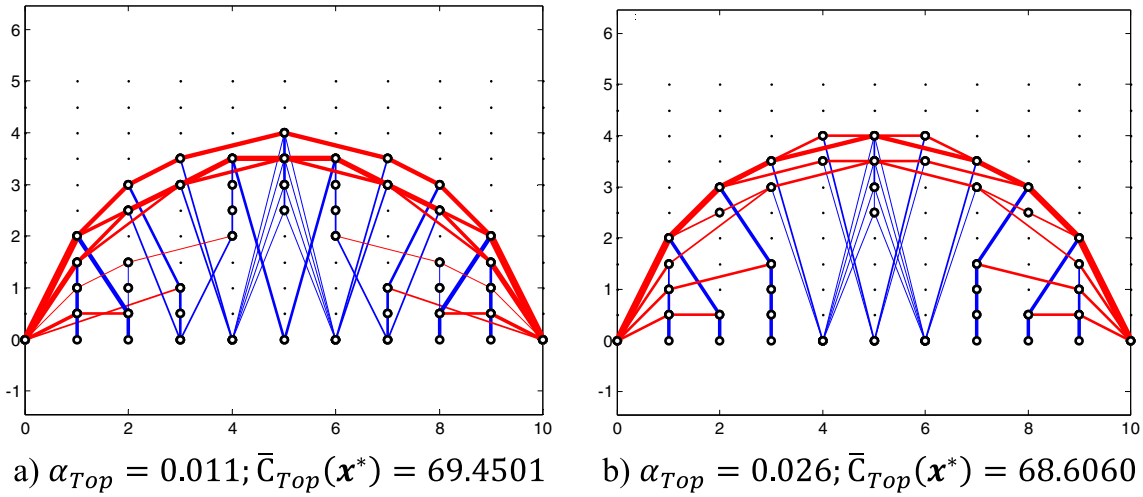

Fig. 18 Move-size (OC γ parameter) dependence on the topology using the filter approach with TR on a full ground structure (11 × 11 grid) considering $\alpha_f = 0.01$ and $\lambda_o = 10^{-8}$: **a** $\gamma = 2$; **b** $\gamma = 6$

equilibrium control ($\gamma = 1/4$), respectively. A comparison of Fig. 22b with Fig. 23b reveals that the former case leads to a FSD, while the latter case does not.

When the control of equilibrium and/or objective function is enforced, then the optimality condition does not hold and the stresses are not constant in the final topology, as shown in Figs. 21b and 23b. Sometimes there are members with very low stresses, however, even in this situation the global equilibrium condition still holds.

5 Concluding remarks and extensions

A long standing problem of the standard ground structure approach is its inability to properly define a valid structural model. This problem has been solved in this paper by means of an effective scheme to filter structures out of ground structures. The implementation was based on a nested elastic formulation for compliance minimization; however, some of the ideas presented here might also be applicable to the plastic formulation (Ohsaki 2011; Zegard and Paulino 2014). Our approach uses physical variables and allows control of the minimum ratio between the minimum and maximum areas in the final topology. It leads to a singular problem which is efficiently solved using a Tikhonov regularization on the structural problem (rather than on the optimization problem). The filter allows a multiple choice solution in which the user can control the global equilibrium residual in the final structural topology and limit variations of the objective function between iterations (e.g., compliance). As a result, an unambiguous discrete solution is obtained where all the bars that belong to the topology have well-defined finite areas. The

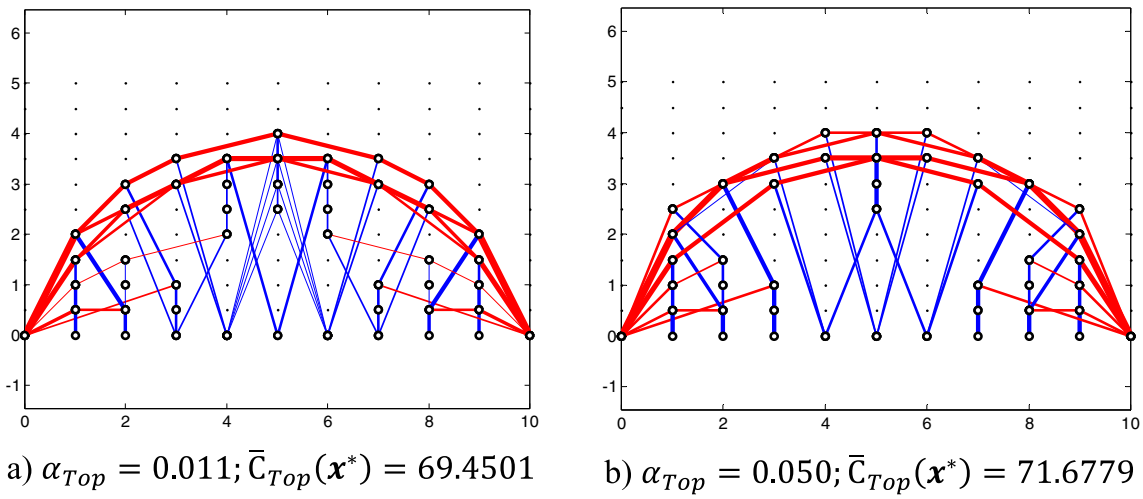

Fig. 19 Tikhonov parameter (λ_o) dependence on the topology using the filter approach with TR on a full ground structure (11 × 11 grid) considering $\alpha_f = 0.01$ and $\gamma = 2$: **a** $\lambda_o = 10^{-8}$; **b** $\lambda_o = 10^{-12}$

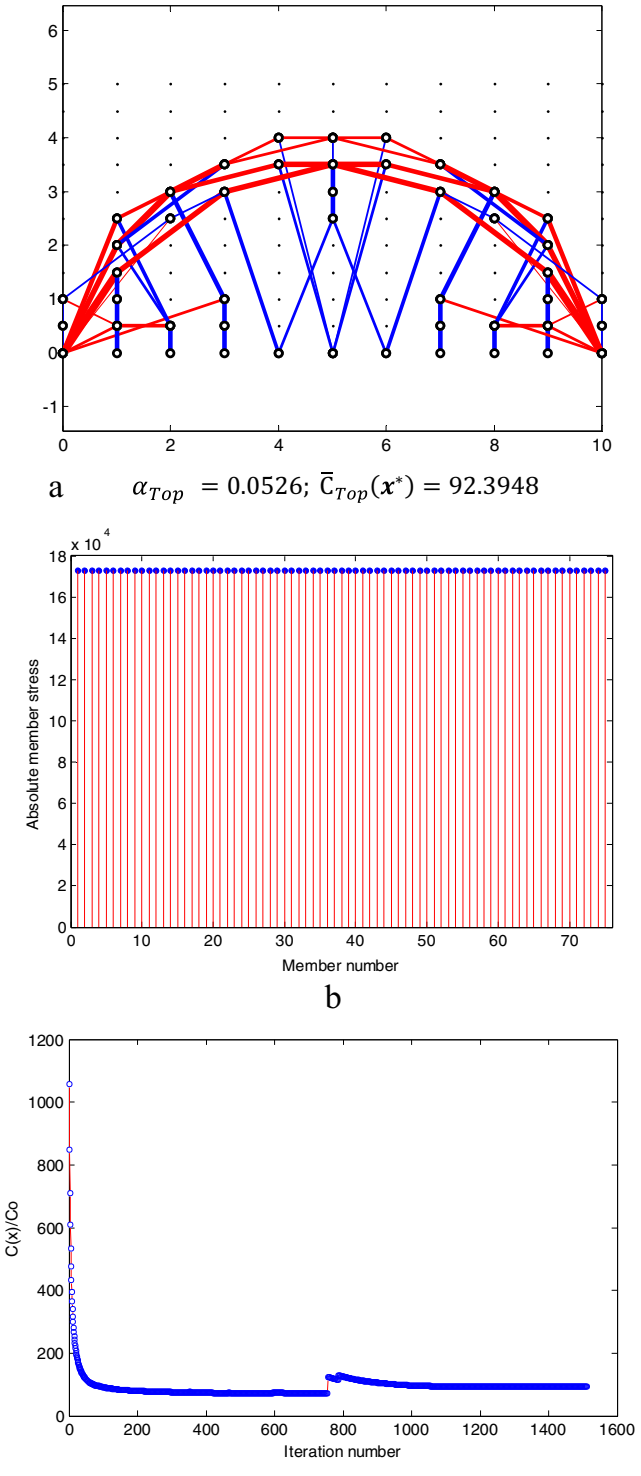

Fig. 20 Filter approach with TR on a full ground structure (11 × 11 grid) for $\alpha_f = 0.03$, $\gamma = 1/4$, $ObjTol = 100$ (no objective control), and equilibrium control considered: **a** final topology, **b** member stress (FSD), and **c** objective function

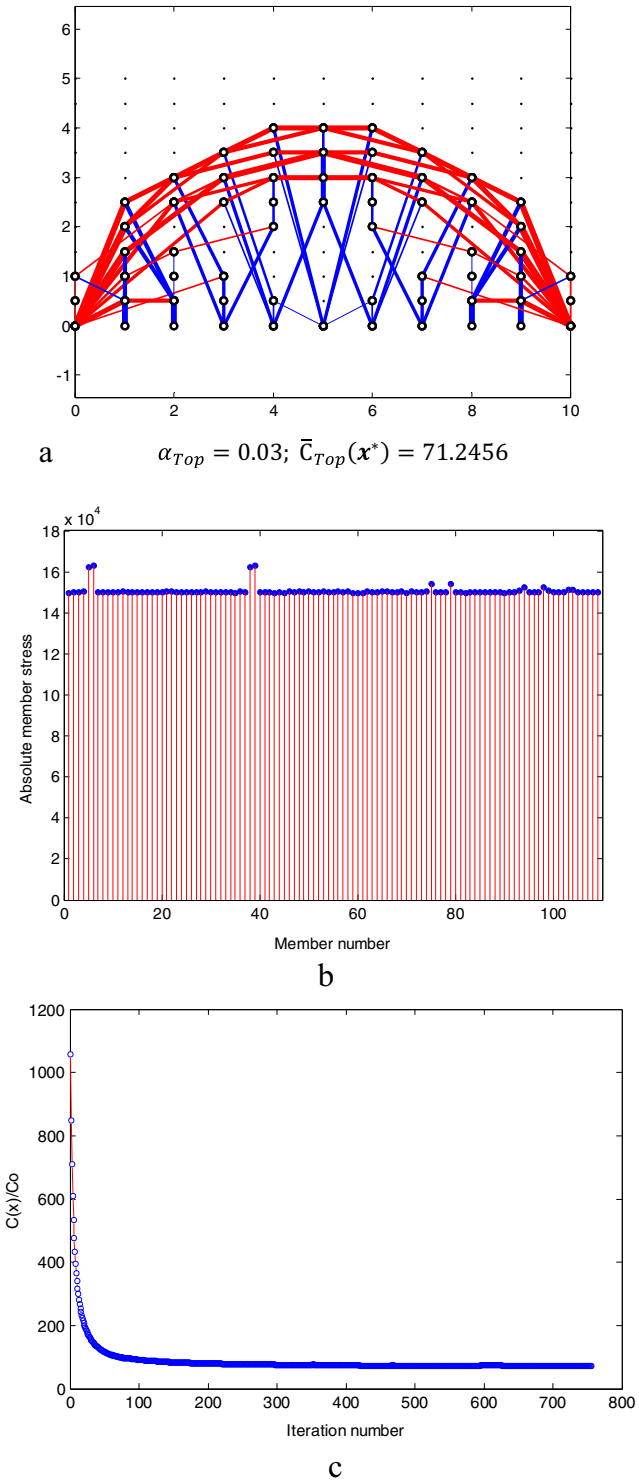

Figure 21 Filter approach with TR on a full ground structure (11x11 grid) for $\alpha_f = 0.03$, $\gamma = 1/4$, $ObjTol = 1$ (objective control considered), and equilibrium control considered: a) final topology, b) member stress (not FSD), and c) objective function

Tikhonov regularization also allows an efficient solution of the convex singular topology optimization problem (Achtziger 1997) without filter – see Fig. 3.

In general, when a higher value of the filter is used, the solution obtained using the present filtering scheme with TR may still be improved in a post-processing stage. Although global equilibrium is guaranteed, hanging bars (i.e., bars that

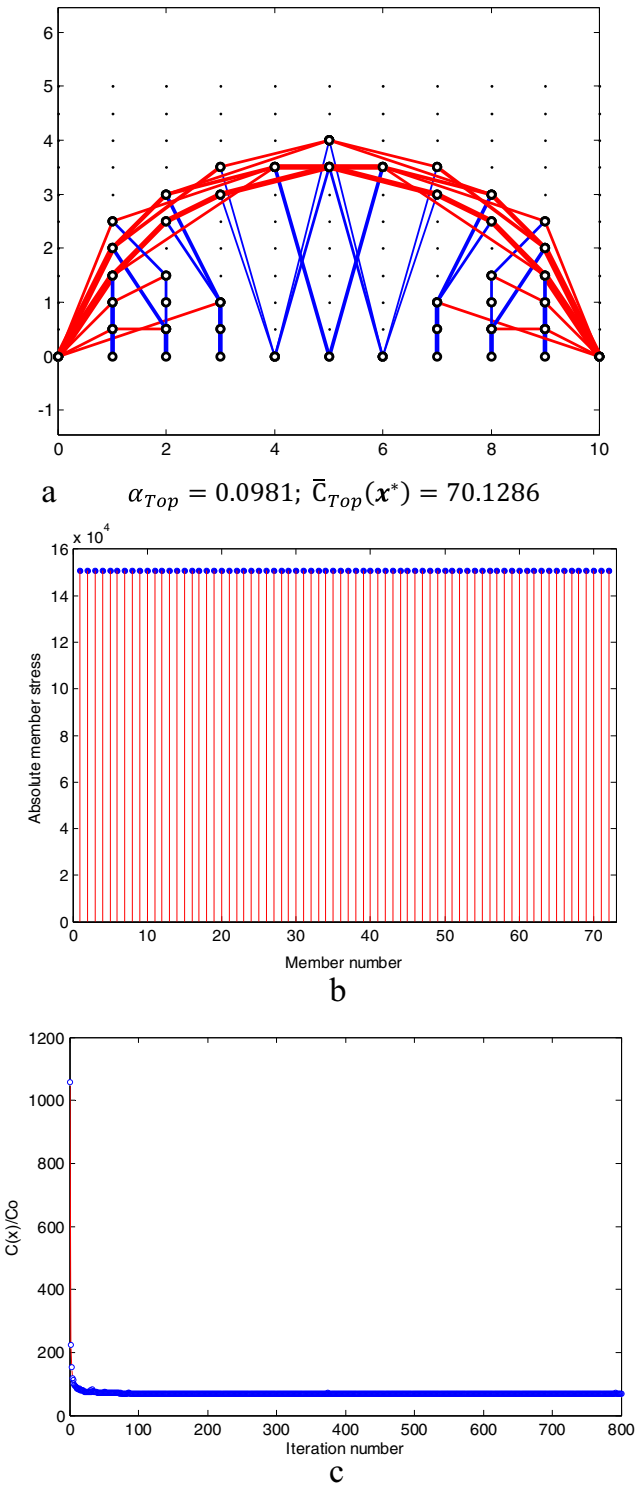

Fig. 22 Filter approach with TR on a full 11 × 11 ground structure for $\alpha_f = 0.06$, $\gamma = 5$, $ObjTol = 100$ (no objective control), and no equilibrium control: **a** final topology, **b** member stresses (FSD), and **c** objective function

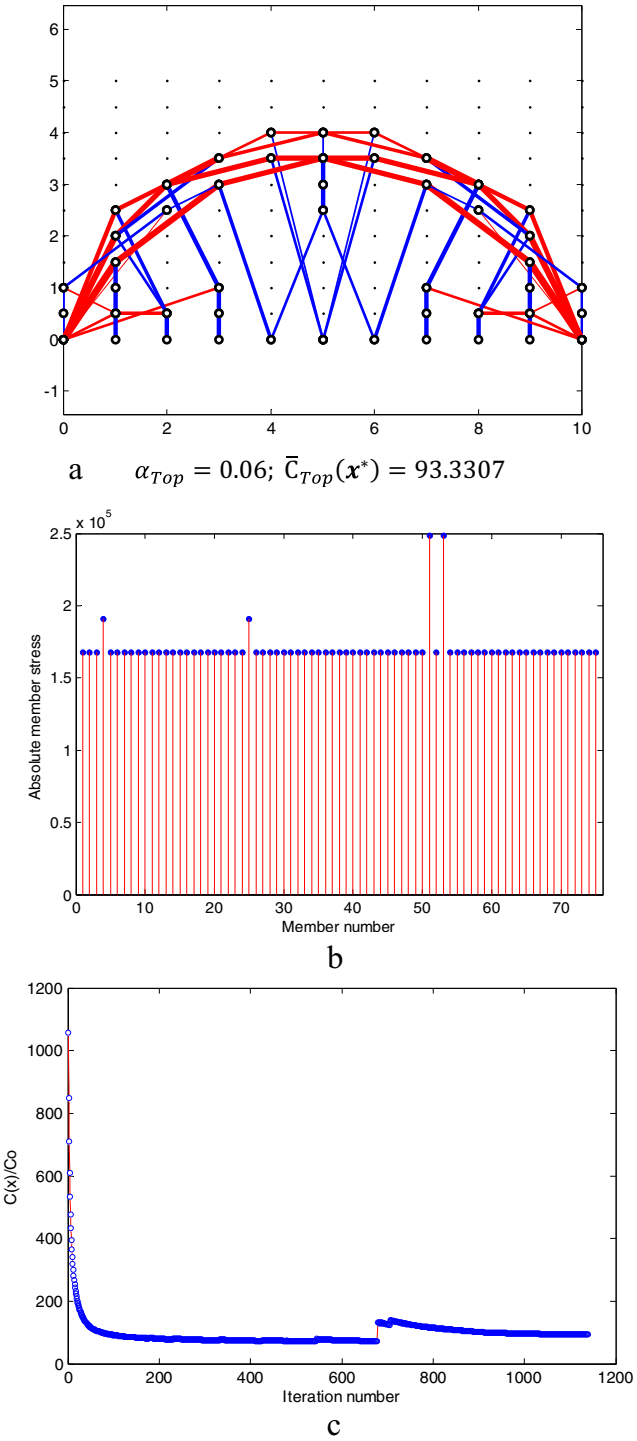

Fig. 23 Filter approach with TR on a full 11 × 11 ground structure for $\alpha_f = 0.06$, $\gamma = 1/4$, $ObjTol = 100$ (no objective control), and equilibrium control considered: **a** final topology, **b** members stresses (not FSD), and **c** objective function

are disconnected from the structure at one or both ends) may occur in the final solution (notice that applied loads were considered in the present work, but not self-weight). However, these hanging bars can be easily tracked and removed from the structure. Another situation that can be handled in a post-processing stage is the occurrence of aligned hinges. Those hinges can also be eliminated in a post-

processing stage. These simple post-processing steps provide better definition of the structural configuration.

As we pointed out, our implementation is based on the OC and thus an artifact of the OC is that the member of null area does not return to the topology (see Section 3). From a practical point of view, the structural engineer might be mostly interested in relatively lower values of the filter. In this scenario, the return of bars is rather infrequent, and thus the use of the OC might be an acceptable approximation. However, in the general case, we could base the optimization scheme on the MMA, which can handle the return of members. This is a topic that deserves further investigation.

It is reasonable to question why this paper emphasizes the elastic formulation, rather than the plastic, especially considering the fact that, for the linear problems presented here, the plastic formulation is much more efficient than the elastic one. Our choice of formulation is based on the aspiration to establish a feasible computational platform that is able to handle a larger class of problems such as those involving nonlinear (material and geometric) behavior. As part of our future work, we intend to extend the present filtering scheme to deal with problems containing nonlinear behavior, which is a class of problems that the plastic formulation cannot handle. In summary, this paper is meant to demonstrate the proposed filter method, and thus considers a simple class of problems in order to not cloud the features of the method. Therefore, we feel that the choice of the elastic formulation over the plastic is justified as this paper addresses some of the major issues with the standard nested elastic approach (i.e., we can extract different topologies, accelerate the solution process, guarantee equilibrium in the final topology, and also enforce the level of the resolution specified by the user) and provides a basic platform for future research and development.

The filtering approach has applications in several areas of topology optimization, such as nonlinear analysis (Bendsoe and Sigmund 2003; Ohsaki 2011), buckling (Zhou 1996; Rozvany 1996; Guo et al. 2005), and reliability based topology optimization or RBTO (Liu 2014). For instance, the filter feature with explicit control on the member areas allows the user to play with different alternatives prior to selecting a specific structural configuration. In standard dynamic problems, once the topology is defined, it might need to be interpreted to define a structural topology without low cross sectional areas. For nonlinear problems, the filter can influence the following aspects: (1) allows removal of potential instabilities in low stiffness regions (difficulty of convergence in this situation); (2) allows check and control of equilibrium and stability in the actual topology; and (3) allows control of the desired level of resolution of the final topology. Finally, large scale RBTO would be desirable considering the filtering scheme both for the optimization iterations and the reliability iterations of the process. These problems are presently under consideration by the authors.

The aforementioned technique to deal with singular problems can lead naturally to other types of filters. For instance, instead of applying the filter at every iteration (as done in the present work), it can be applied at different intervals of the iterative process or just once at the end of the iterative process.

We end this paper with a few words regarding our understanding of singular solutions (see Section 2.4) and vision to the field, especially from an educational perspective. Traditionally, singularity has been a topic that has been avoided in the field of structural engineering. However, as motivated by the present work, the treatment of structural problems by means of efficient singular solutions, is a promising field to be exploited further and that holds the key for further understanding and advances in the field.

Acknowledgments We acknowledge the financial support from the Brazilian agency CNPq (National Council for Research and Development), from the Laboratory of Scientific Computing and Visualization (LCCV) at Federal University of Alagoas (UFAL), and from the US National Science Foundation (NSF) through Grants CMMI #1321661 and CMMI #1335160. We are also grateful to the endowment provided by the Raymond Allen Jones Chair at the Georgia Institute of Technology. In addition, we thank Emily R. Daniels and Ke Liu for insightful discussions which significantly enriched the manuscript. The information presented in this paper is the sole opinion of the authors and does not necessarily reflect the views of the sponsoring agencies.

Appendix A – Nomenclature

α_i, η, M	Optimality criteria parameters
α_f	Filter size
α_{Top}	Resolution of the structural topology
ϵ	Small positive number
γ	Move size parameter
ρ	Global equilibrium tolerance
λ, λ_o	Tikhonov regularization parameters
Ω	Potential energy of external loads
Π	Total potential energy
$\boldsymbol{A}_n$	Member n incidence kinematic matrix
E	Elasticity modulus
$\boldsymbol{F}$	Force vector
$\boldsymbol{F}_{Top}$	Force vector in the structural topology
C	Objective function
$\overline{C}$	Normalized objective function
$\boldsymbol{K}$	Global stiffness matrix
$\boldsymbol{K}_{Top}$	Global stiffness matrix for the structural topology
$\boldsymbol{k}^{(i)}$	Stiffness matrix for member i in local coordinate
ℓ	Member length

$\boldsymbol{L}$	Vector of the member length
M	Move limit (optimality criteria)
N	Number of members
tol	Tolerance in the OC
$ObjTol$	Tolerance in the objective function between iterations
$\boldsymbol{u}$	Displacement vector
$\boldsymbol{u}_{eq}$	Displacement vector at the equilibrium configuration
$\boldsymbol{u}_n$	Member n displacement vector
$\boldsymbol{u}_{Top}$	Displacement vector in the structural topology
$\boldsymbol{V}$	Eigenvectors of $\boldsymbol{K}$
$\mathbf{v}_i$	Eigenvector i of $\boldsymbol{K}$
U	Strain energy
V_{max}	Maximum volume
$\mathscr{R}$	Range
$\mathbb{R}$	Set of real numbers
x_j^{min}, x_j^{max}	Lower and upper bounds for member cross-sectional area

Appendix B – Global equilibrium error

In this Appendix, we compare the values of the compliance and the global equilibrium error obtained with the Moore-Penrose Inverse, least squares with Tikhonov regularization ($\lambda_o = 10^{-8}$), and the total potential energy with Tikhonov regularization ($\lambda_o = 10^{-8}$) for solution of ill conditioned systems. The source of ill conditioning here is the occurrence of significantly different cross-sectional areas in the resulting topology, as illustrated by Fig. 24.

Table 7 shows that when $\epsilon = 0.01$, the values of compliance (C) and particular solution ($\boldsymbol{u}_p$) for the three approaches are similar. On the other hand, Table 8 shows that when $\epsilon = 0.001$, the values of compliance and particular solution ($\boldsymbol{u}_p$) for the pseudo inverse and the potential energy with Tikhonov regularization are similar, however, such is not the case for the least squares solution, which also displays a large equilibrium residual.

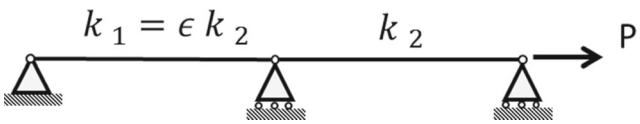

Fig. 24 Ill conditioned stiffness matrix for $\epsilon < 1$

Table 7 Nonsingular ($\epsilon = 0.01$; $k_2 = 10kN/m$; P = 10 kN)

Method	$\boldsymbol{u}_p$	$C = \boldsymbol{F}^T\boldsymbol{u}_p$	$\lvert\boldsymbol{K}\boldsymbol{u}_p - \boldsymbol{F}\rvert/\lvert\boldsymbol{F}\rvert$
Moore-Penrose Inverse (MP)	{100.0000 101.0000}	$1.010\ 10^3$	$3.2155\ 10^{-14}$
Least square + TR	{99.9191 100.9187}	$1.009\ 10^3$	$5.7235\ 10^{-4}$
Potential Energy + TR	{99.9998 100.9998}	$1.010\ 10^3$	$1.4284\ 10^{-6}$

Table 8 Nonsingular ($\epsilon = 0.001$; $k_2 = 10kN/m$; P = 10 kN)

Method	$\boldsymbol{u}_p$	$C = \boldsymbol{F}^T\boldsymbol{u}_p$	$\lvert\boldsymbol{K}\boldsymbol{u}_p - \boldsymbol{F}\rvert/\lvert\boldsymbol{F}\rvert$
Moore-Penrose Inverse (MP)	{1.0000 1.0001} 10^3	$1.0010\ 10^4$	$1.8190\ 10^{-13}$
Least square + TR	{9.2583 9.2680} 10^3	$9.2680\ 10^3$	0.0524
Potential Energy + TR	{1.0000 1.0010} 10^3	$1.0010\ 10^4$	$1.4156\ 10^{-5}$

Appendix C – Iterative scheme for solving singular systems of equations

In this Appendix, we present a practical iterative solution for the singular system defined by (10). The ideas presented here are based on Roonau and Parsons (1995). Adding the factor $\lambda\,\boldsymbol{u}$ in both sides of (10), we obtain

$$(\boldsymbol{K} + \lambda\,\boldsymbol{I})\,\boldsymbol{u} = \boldsymbol{F} + \lambda\,\boldsymbol{u} \tag{42}$$

where λ is a small number (e.g., $\lambda_o = 10^{-4}$ to 10^{-12} times the mean of the diagonal of $\boldsymbol{K}$) that removes the singularity of the stiffness matrix $\boldsymbol{K}$ and provides faster convergence. We obtain the solution using an iterative algorithm in the form

$$(\boldsymbol{K} + \lambda\,\boldsymbol{I})\,\boldsymbol{u}^{(k+1)} = \boldsymbol{F} + \lambda\,\boldsymbol{u}^{(k)} \tag{43}$$

Now we obtain a particular solution of the singular system of equations which, from a numerical point of view, is independent of the parameter λ. The convergence is obtained using a tolerance on the displacement, e.g., $|\boldsymbol{u}^{(k+1)} - \boldsymbol{u}^{(k)}| \le 10^{-7}\ |\boldsymbol{u}^{(k)}|$. To illustrate the method, Fig. 19b of Example 2 is solved with this approach and the results obtained are presented in Fig. 25 and Table 9. The new results illustrate convergence toward the same topology of Fig. 19b, Moreover, the equilibrium error is relatively small for all values of the parameter λ.

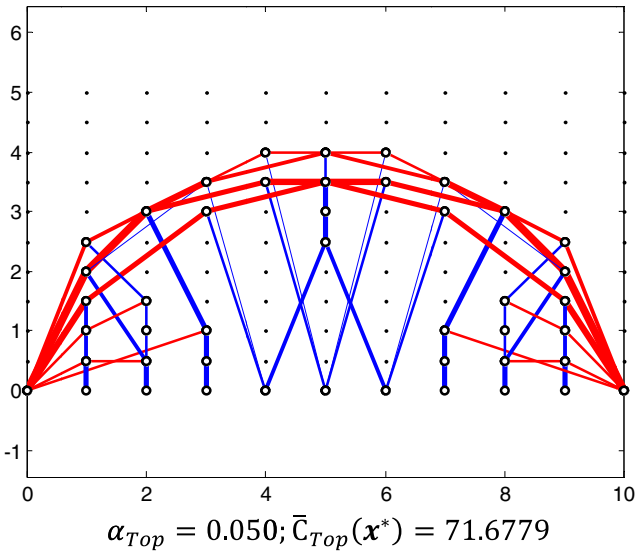

Fig. 25 Dependence of the topology on the Tikhonov parameter using the filter approach on a full ground structure (11 × 11 grid) with $\alpha_f = 0.01$ and $\gamma = 2$ for both the approach of Section 2.7 with $\lambda_o = 10^{-12}$ and the iterative approach with $\lambda_o = 10^{-4}; 10^{-5}; 10^{-6}; 10^{-8}$

Table 9 Number of iterations, objective function, and equilibrium error for different values of λ_o

λ_o	Number of iterations	$\overline{C}_{Top}(x^*)$	$\lvert Ku_p - F\rvert/\lvert F\rvert$
10^{-4}	461	71.6779	8.0710^{-8}
10^{-5}	464	71.6779	4.0310^{-11}
10^{-6}	471	71.6779	2.6310^{-12}
10^{-7}	355	69.7218	5.1910^{-15}
10^{-8}	451	71.6779	1.5110^{-14}

Appendix D – Filtering out mapping example

In this section we show a simple example demonstrating how the force vector and stiffness matrix corresponding to the topology can be mapped from those corresponding to the ground structure, based on the equations outlined in Section 2.3. Figure 26 shows the load and support conditions (a), the ground structure degrees of freedom (b), and the topology degrees of freedom (c).

The force vector and the stiffness matrix for the ground structure are given by

$$\boldsymbol{F} = P\begin{Bmatrix} 0 \\ -1 \\ 1 \end{Bmatrix} \tag{44}$$

$$\boldsymbol{K} = \begin{bmatrix} k_3 & -k_3 & 0 \\ -k_3 & k_2 + k_3 & -k_2 \\ 0 & -k_2 & k_1 + k_2 \end{bmatrix} \tag{45}$$

The transformation matrix from topology displacements to ground structure displacements ($\boldsymbol{u} = \boldsymbol{T}\,\boldsymbol{u}_{Top}$) is given by

$$\boldsymbol{T} = \begin{bmatrix} 0 & 0 \\ 0 & 1 \\ 1 & 0 \end{bmatrix} \tag{46}$$

Now we can obtain the force vector and stiffness matrix for the topology using

$$\boldsymbol{F}_{Top} = \boldsymbol{T}^T\boldsymbol{F} = P\begin{Bmatrix} 1 \\ -1 \end{Bmatrix} \tag{47}$$

$$\boldsymbol{K}_{Top} = \boldsymbol{T}^T\boldsymbol{K}\boldsymbol{T} = \begin{bmatrix} k_2 + k_1 & -k_2 \\ -k_2 & k_2 + k_3 \end{bmatrix} \tag{48}$$

Considering the null stiffness coefficient k_1 and k_3, we obtain the singular stiffness matrix for the topology

$$\boldsymbol{K}_{Top} = \begin{bmatrix} k_2 & -k_2 \\ -k_2 & k_2 \end{bmatrix} \tag{49}$$

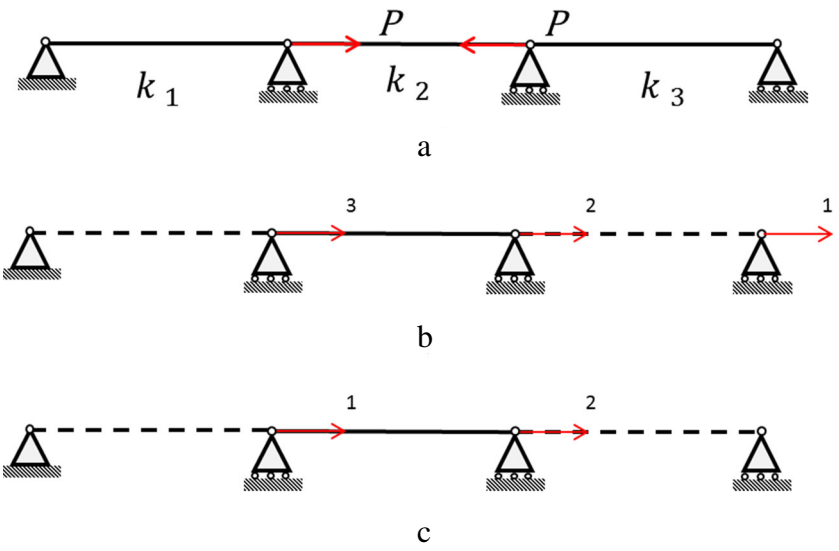

Fig. 26 **a** Loading and support conditions; **b** Ground structure degrees of freedom ($\boldsymbol{K}\boldsymbol{u} = \boldsymbol{F}$); **c** Topology degrees of freedom ($\boldsymbol{K}_{Top}\boldsymbol{u}_{Top} = \boldsymbol{F}_{Top}$). Note: *Dashed lines* denote null stiffness

References

Achtziger W (1997) Topology optimization of discrete structures: an introduction in view of computational and nonsmooth aspects. In: Rozvany GIN (Ed) Topol. Optim. Struct. Mech. (pp. 57–100). Springer,Wien

Bendsoe MP, Sigmund O (2003) Topology optimization: theory, methods, and applications. Springer Verlag

Ben-Israel A, Greville TNE (2003) Generalized inverses - theory and applications, 2nd edn. Springer Verlag, New York

Bruns TE (2006) Zero density lower bounds in topology optimization. Comput Methods Appl Mech Eng 196(1–3):566–578

Christensen PW, Klarbring A (2009) An introduction to structural optimization. Springer, Linköping

Engl HW, Hangke M, Neubauer A (1996) Regularization of inverse problems. Kluwer Academic Publishers

Farhat C, Géradin M (1998) On the general solution by a direct method of a large-scale singular system of linear equations: application to the analysis of floating structures. Int J Numer Methods Eng 41(4):675–696

Gaynor AT, Meisel NA, Williams CB, Guest JK (2014) Multiple-Material Topology Optimization of Compliant Mechanisms Created Via PolyJet Three-Dimensional Printing. J Manuf Sci Eng 136(6): 61015, ASME

Ge Q, Qi HJ, Dunn ML (2013) Active materials by four-dimension printing. Appl Phys Lett 103(13):2011–2016

Groenwold AA, Etman LFP (2008) On the equivalence of optimality criterion and sequential approximate optimization methods in the classical topology layout problem. Int J Numer Methods Eng 73:297–316

Guo X, Cheng GD, Olhoff N (2005) Optimum design of truss topology under buckling constraints. Struct Multidiscip Optim 30:169–180

Liu K (2014) Segmental multi-point linearization for topology optimization and reliability analysis. MSc Thesis. Univiersity of Illinois at Urbana-Champaign, Urbana

Ohsaki M (2011) Optimization of Finite Dimensional Structures (p. 425). CRC Press, Boca Raton

Ramos Jr. AS, Paulino GH (2015) Convex topology optimization for hyperelastic trusses based on the ground-structure approach. Struct Multidiscip Optim 51(2):287–304

Roonau A, Parsons ID (1995) Suppressing Singularities when Computing Critical Points Using Multigrid Methods. Comput Mech 95:1517–1522

Rozvany GIN (1996) Difficulties in truss topology optimization with stress, local buckling and system stability constraints. Struct Optim 11:213–237

Svanberg K (1987) The method of moving asymptotes—a new method for structural optimization. Int J Numer Methods Eng 24:359–373

Tikhonov AN, Arsenin VY (1977) Methods for solving Ill-posed problems. Wiley, New York

Wang S, de Sturler E, Paulino G (2007) Large scale topology optimization using preconditioned Krylov subspace methods with recycling. Int J Numer Methods in Eng 69:2441–2468

Washizawa T, Asai A, Yoshikawa N (2004) A new approach for solving singular systems in topology optimization using Krylov subspace methods. Struct Multidiscip Optim 28:330–339

Yanai, H., Takeuchi, K., Takane, Y. (2011) Projection Matrices, Generalized Inverse Matrices, and Singular Value Decomposition. Springer-Verlag, New York

Zegard T, Paulino GH. Bridging topology optimization and additive manufacturing. Struct Multidisc Optim. Accepted. doi 10.1007/s00158-015-1274-4

Zegard T, Paulino GH (2014) GRAND - Ground structure based topology optimization for arbitrary 2D domains using MATLAB. Struct Multidisc Optim 50(5):861–882

Zhou M (1996) Difficulties in truss topology optimization with stress and local buckling constraints. Struct Optim 11:134–136